

Precoder for Multimode Optical Fiber Under a Low Modal Coupling Assumption

---

A Thesis

Presented to  
the faculty of the School of Engineering and Applied Science  
University of Virginia

---

in partial fulfillment  
of the requirements for the degree

Master of Science

by

Sara H. Davis

August

2015

APPROVAL SHEET

The thesis  
is submitted in partial fulfillment of the requirements  
for the degree of  
Master of Science

---

AUTHOR

The thesis has been read and approved by the examining committee:

---

Advisor

Dr. Maïté Brandt-Pearce

---

---

Dr. Stephen Wilson

---

---

Dr. Andreas Beling

---

Accepted for the School of Engineering and Applied Science:



Dean, School of Engineering and Applied Science

August  
2015

# Abstract

High speed and bandwidth applications have become more popular and available within recent years, shifting network traffic from voice-based to data-based traffic. Fiber optic communications have made increased network capacity substantially and made such growth possible. However, it is expected within the next 5 years that the capacity of classic single-mode optical fiber systems will be reached. Several groups have attempted to enhance single-mode fiber capacity via increased modulation constellation points or adopting coherent detection, but such techniques are only temporary solutions to the capacity crunch problem. Conversely, many groups are turning toward revolutionizing lightwave systems by adapting multimode fibers for long-haul applications, where multiple modes carry several bit streams down the fiber and leave the potential to increase capacity substantially.

Despite the opportunity for large capacity gains, multimode fiber performance is inherently hindered by modal dispersion and modal coupling. The several modes in the fiber travel at different speeds and, therefore, do not reach the receiver at the same time, which causes intersymbol interference and the system to be described as frequency selective in nature. Additionally, modal coupling causes power transfer between modes and worsens performance to unacceptable levels. Several groups have attempted to utilize multimode fiber potential via post-processing methods or transmission of select modes of the fiber with moderate success. However, little work has been done in precoding, which would eliminate the need for expensive coherent reception and maximize channel performance. Precoding requires the adoption of a Mach-Zehnder modulation, an inexpensive option to improve multimode fiber performance.

In this thesis, the concept of precoding was explored for a three mode low coupling system through an iterative training scheme that sends coefficients back to the transmitter. By

sending specific training sequences through the transmission channel, the magnitude and phase information of the system can be exploited and subsequently used to develop a precoder that is nearly identical to the inverse of the transmission matrix. Particularly when additive white Gaussian noise is present and at low SNRs, we propose that several realizations of an estimate of the inverted channel matrix are generated and subsequently averaged in order to create a generalized precoder.

We demonstrate that the precoder produced is an accurate reproduction of the inverted channel matrix, which is the ideal precoder. The maximum mean squared error found between coefficients was relatively low, with most precoder coefficient errors hovering in the order of tenths of error. Additionally, we demonstrate that precoding in the low coupling regime improves performance greatly, particularly with regards to the secondary modes of the system, and is tolerant to modal crosstalk as the number of iterations increases. However, as the amount of modal coupling increases and the channel becomes frequency selective, the precoder becomes less effective.

We conclude that the precoder developed thrives when operated on multimode fibers with low coupling, which describes a system that is frequency flat, and reproduces an accurate estimate of the ideal precoder. Concepts for a precoder for the high coupling scenario are discussed and left as future work.

*In loving memory of my aunt and uncle, Anne Allen and Salvatore Pepe*

# Acknowledgements

First and foremost, I would like to thank Dr. Maïté Brandt-Pearce, my advisor, for her guidance, support, and patience while completing this thesis. She helped me overcome every obstacle I met throughout my time at UVA without hesitation and knew every step I needed to take next when I hit roadblocks, particularly toward the end of this work. I truly enjoyed working with her and will be forever grateful for her excellent mentoring and remarkable ideas during my graduate career.

I would also like to thank Dr. Stephen Wilson and Dr. Andreas Beling for serving on my committee. Both professors taught me a great deal about communications theory and fiber optics, and I have walked away from their guidance with great confidence in my abilities as a communications engineer.

Of course, none of this would have been possible without the love and support of my friends, both at UVA and from elsewhere. I would like to thank in a very special way the members of the Optical Multiuser/Multichannel Communications group and all my friends in offices C246 and C249 for their help and friendship. Additionally, many thanks go toward Ali Chaudhry for his companionship and reassurance during my time at UVA. I'd also like to thank my dear friends, Lauren Cahill, Brad Ebinger, and Chris Franzwa, for their unending friendship, support, and laughs throughout my educational career.

Finally, I would like to thank my mother, father, and sister, Adriana, for their unconditional love and encouragement. It is with their love that made this thesis both conceivable and meaningful, and I could never thank them enough for the support and guidance they have given me since my childhood.

# Contents

<b>1 Introduction</b>	<b>1</b>
1.1 Current System Capacity and Potential Enhancements.....	2
1.2 Introduction to Multimode Optical Fiber.....	9
1.3 Utilizing Multimode Fiber Potential.....	10
1.4 Thesis Outline.....	10
1.5 Chapter Summary.....	11
<b>2 System Model</b>	<b>9</b>
2.1 Transmitter.....	10
2.2 Precoder.....	11
2.3 Multimode Optical Fiber.....	12
2.4 Receiver.....	13
2.5 System Performance Evaluation.....	14
2.6 Chapter Summary.....	15
<b>3 Channel Model</b>	<b>16</b>
3.1 Ideal Propagation Modeling.....	17
3.2 Modal Coupling Modeling.....	19
3.3 MMF Channel Analysis.....	20
3.4 Comparison to Other MMF Models.....	35
3.5 Chapter Summary.....	36

<b>4 Precoder Construction and Performance</b>	<b>37</b>
4.1 Precoding Filter Training Scheme.....	39
4.2 Simulation Results.....	45
4.3 Chapter Summary.....	50
<b>5 Summary and Future Work</b>	<b>52</b>
5.1 Thesis Summary.....	52
5.2 Future Work.....	53
<b>6 Bibliography</b>	<b>55</b>

# List of Acronyms

AWGN: Additive white Gaussian Noise

BER: Bit error rate

CSI: Channel state information

DD: Direct detection

EDFA: Erbium doped fiber amplifier

EOP: Eye opening penalty

ISI: Intersymbol interference

LP: linearly polarized

MIMO: Multiple-input multiple-output

MMF: Multimode fiber

MSE: Mean squared error

MZM: Mach-Zehdner Modulator

OFDM: Orthogonal frequency division multiplexing

OOK: On-off Keying

QAM: Quadrature amplitude modulation

RZ: Return to zero

SNR: Signal to Noise Ratio

WDM: Wavelength division multiplexing

# List of Figures

1.1 ISI and pulse broadening as a result of modal dispersion in an MMF .....	4
1.2 A comparison between wireless and MMF communication channels, where H represents the channel matrix.....	5
2.1 MMF system model.....	10
2.2 The super Gaussian pulse shaped filter used in this work where $m = 3$ .....	11
3.1 An MMF divided into sections of equal length, $L_m$ .....	16
3.2 Misalignment between MMF sections with regards to radial offset and rotation angle.....	20
3.3 Magnitude spectra for each mode of MMF with low coupling.....	21
3.4 Phase spectra for each mode of MMF with little coupling.....	22
3.5 Impulse response for each mode of MMF with little coupling.....	23
3.6 Magnitude spectra for each mode of MMF with high coupling.....	25
3.7 Phase spectra for each mode of MMF with high coupling.....	26
3.8 Impulse response for each mode of MMF with high coupling.....	27
3.9 The eye diagram of the LP01 mode when the splice mismatch is 0.01.....	28
3.10 The eye diagram of the LP11a mode when the splice mismatch is 0.01.....	29
3.11 The eye diagram of the LP11b mode when the splice mismatch is 0.01.....	30
3.12 The eye diagram of the LP01 mode when the splice mismatch is 0.05.....	31
3.13 The eye diagram of the LP11a mode when the splice mismatch is 0.05.....	32
3.14 The eye diagram of the LP11b mode when the splice mismatch is 0.05.....	33
3.15 The EOP of each mode as a function of coupling loss.....	34
4.1 Feedback scheme used to predistort each bit stream into the MMF.....	37
4.2 The MSE between the precoder and the inverse of the center frequency transmission matrix.....	43

4.3 The performance curves of the unfiltered and precoded MMFs versus SNR.....	45
4.4 Performance curves comparing the generated and ideal precoders.....	46
4.5 LP11a precoder performance vs SNR as a function of the number of iterations.....	47
4.6 LP11b precoder performance vs SNR as a function of the number of iterations.....	48
4.7 Precoder performance across various levels of splice mismatching.....	49

# List of Tables

1.1 A comparison of signal processing methods.....	7
--	---

# Chapter 1 - Introduction

The demand for both high speed and bandwidth applications has grown substantially in recent years. Beginning in the mid-2000s, network traffic has seen a shift from primarily voice-based to data-based traffic, due in part to the increasing availability of high bandwidth applications such as video chatting, cloud computing, and others, resulting in traffic growths by nearly 50 to 60% each year [1]. Traditional copper communication lines suffer from high attenuation and inherently low bandwidth, and consequently cannot support such network exchanges properly. Instead, the communications community has redirected efforts toward fiber optic communication systems in order to support the demand for data. Fiber optic, also known as lightwave, systems offer many advantages over traditional copper lines, including low attenuation loss, lower maintenance costs, and a significant theoretical bandwidth [2].

The immense potential gains offered by fiber optic systems had been considered in the early 1960's, but did not become a reality until fairly recently. Beginning in the 1970's, fiber optics cables with low attenuation loss and single-frequency light sources came into fruition, creating a massive push for research in the area. Lightwave systems began to be commercially available and deployed in the 1980's, with small core diameter, single-mode fibers being the medium of choice [3]. The enormous capacity offered by fiber optics has since then been exploited, particularly with the introduction of erbium-doped fiber amplifiers (EDFAs) and wavelength-division multiplexing (WDM), and is continually being pushed by researchers. Laboratory experiments performed in the early 2010's have shown lightwave systems to be able to transmit tens and hundreds of terabits of data with little distortion [2].

## 1.1 Current System Capacity and Potential Enhancements

Despite the incredible gains made in communications, classic lightwave systems are beginning to reach their maximum capacity. Initially, dispersion was the critical limiter on fiber capacity, but has since become negligible with the introduction of various dispersion management methods in the 1990's [2]. The primary limiting factor to fiber capacity is nonlinearities incurred during propagation. Fiber nonlinearities worsen with fiber length and higher data rates, and have definitively slowed capacity enhancing research and eventual commercial deployment within the last 10 years. Capacity projections estimate that the classic fiber optic systems as they exist currently will reach their ultimate capacity in the year 2020, a mere 5 years on the horizon [4].

In response, researchers are probing several avenues to increase capacity for the current fiber systems. One potential option is to enhance the number of modulation constellation points to increase capacity gains, i.e. 16 quadrature amplitude modulation (QAM) and beyond. However, an extremely high number of points are required to yield a meaningful gain in capacity, which in turn increases complexity considerably and is not practical in the long run [2]. Another potential solution is to adopt orthogonal frequency-division multiplexing (OFDM) for optical systems, where data is encoded on several carrier frequencies. A clear advantage to OFDM is that a lower number of constellation points for modulation would be necessary, which would ultimately reduce complexity. However, the downside of OFDM is that the underlying modulation method for the system would still be limited by the same constraints as a single carrier system, making it difficult to achieve significant capacity gains as well [2]. Another avenue of exploration exists in multicore fibers, where a fiber optic cable contains several single mode fiber cores. However, multicore fibers face performance issues principally due to crosstalk

between cores. Finally, several groups have taken an interest in applying coherent detection at the receivers for metro or access networks, with the drawback being increased complexity without high capacity gains in the long run [4].

## **1.2 Introduction of Multimode Optical Fiber**

Clearly, standard single-mode optical fibers are reaching their ultimate capacity, forcing researchers to consider various configurations to overhaul current lightwave systems altogether. A developing field of interest is to develop optical systems that accommodate multimode fibers (MMFs), where more than one guided mode propagates through the fiber at once. The physical difference between single-mode and multimode fibers is the latter has a larger fiber core diameter, allowing the cable to guide several light rays. The larger core itself yields many benefits to lightwave systems, one of which is reducing issues associated with fiber nonlinearities [2]. MMFs are typically more cost effective to install and maintain as well. Single-mode fibers have core diameters of only several microns, versus MMFs whose core diameters are tens of microns. A small core diameter requires precise alignment in splicing, which complicates and raises costs of packaging [5].

MMFs present a significant opportunity to enhance fiber capacity and meet network traffic demands. The concept of operation behind MMFs is that each mode traveling down the fiber would carry a different bit stream. Assuming that the modes are independent of each other, the system capacity can, therefore, be increased by the number of guided modes existent in the fiber [6]. Since complexity increases with the number of modes, most research has focused on the development of few mode fibers, i.e. fibers with two or three modes propagation at one time.

Initially, MMFs were considered to be the fiber of choice for lightwave systems. Researchers originally had concerns regarding the size of single-mode fibers in commercial deployment. However, single-mode fibers came into favor beginning in the 1980's, when long distance communications became open to competitive carriers, and therefore becoming the fiber of choice for many years, principally in long distance applications [4]. MMFs, instead, became common and are still used heavily only in short distance links, such as data centers, office buildings, and other applications, primarily due to the effects of modal dispersion [5].

The key impairment to MMF research and commercial deployment for long distance applications is modal dispersion, a phenomenon illustrated in Figure 1.1. Due to fiber geometry, modal dispersion occurs because the different modes will travel at different velocities and take different propagation paths while migrating through an MMF. Each mode will incur varying propagation delays and, therefore, will not reach the receiver at the same time, causing pulses to spread in time in an occurrence known as intersymbol interference (ISI). Additionally, the bit streams carried by each mode overlap with one another during propagation in a process known as modal mixing. Both phenomena combined cause high and low bits to become indistinguishable from each other, leading to high bit error rates (BERs) [6]. When considering long distances, modal dispersion present in MMFs cause the channel to become frequency selective in nature, meaning that it contains filtering effects and complicates system development considerably [7].

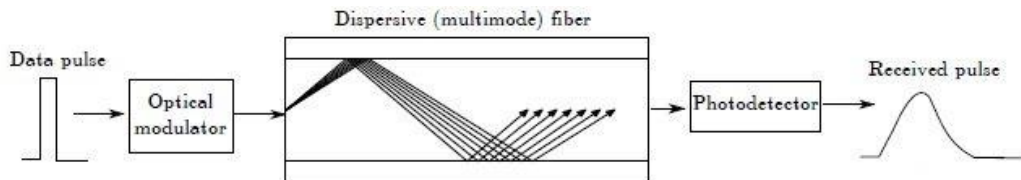


Figure 1.1: ISI and pulse broadening as a result of modal dispersion in an MMF [5].

### 1.3 Utilizing Multimode Fiber Potential

During the initial phases of optical fiber development, little could be done in terms of alleviating the effects of ISI, and MMFs fell to the wayside in favor of single-mode fibers. In recent years, however, substantial strides in signal processing and communications techniques have granted an opportunity to create a powerful MMF system. A noteworthy avenue lies in multiple-input and multiple-output (MIMO) methods used in wireless communications, where several transmit and receive antennas are employed to achieve multiplexing gains [8]. MIMO research has blossomed since its inception, ranging from various applications in wireless settings to adaptations in other systems, especially in MMFs as depicted in Figure 1.2. The key concept of MIMO for MMFs is that multiple transmitters and receivers are used in a similar fashion to increase capacity gains, where the multiple modes are considered to be propagation degrees of freedom.

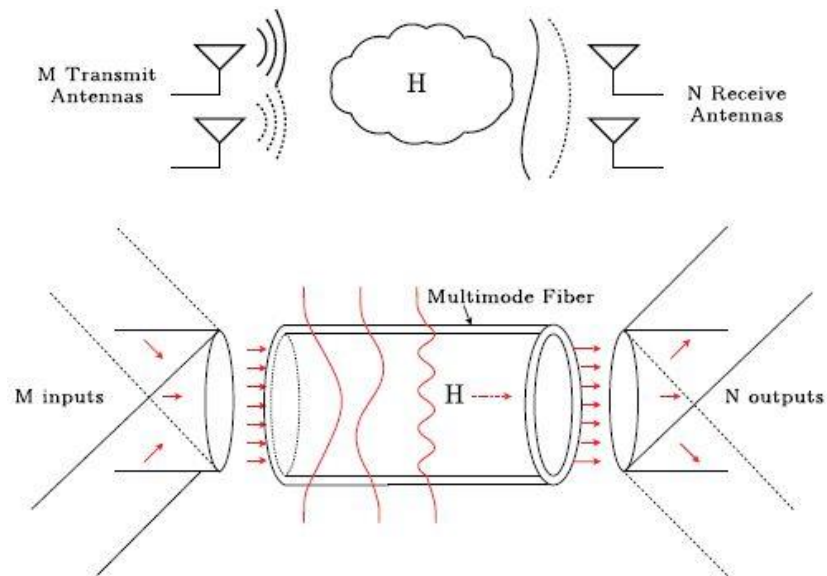


Figure 1.2: A comparison between wireless and MMF communication channels, where  $H$  represents the channel matrix [5].

Concurrently, signal processing technology and methods have evolved to the point of supporting real time applications, thus becoming the principal area of research in alleviating ISI in MMFs [8]. Three key signal processing methods exist and are summarized in Table 1.1. One potential realization is to equalize ISI effects at the receiver, in the form of post-processing. The obvious advantage to receiver equalization is that the channel information can be readily determined and, thus, allow the signal to be corrected properly. However, receiver processing may require costly coherent detection, as opposed to the traditional inexpensive direct detection used in optical systems [9]. Several groups have also contemplated the idea of launching signals over different modes of the fiber that are more tolerant to modal dispersion. Ideally, such a technique would eliminate the need for transmitter or receiver processing altogether. However, researchers are instead finding that transmitting different types of modes holds no great advantage, since ISI is not substantially diminished without pre- or post-processing [6].

A relatively unexplored option to enhance MMF capacity is to apply precoding at the transmitter, thus eliminating ISI at the transmitter before each mode is launched. Precoding is a method where the signal is coded using channel state information (CSI) prior to transmission [8]. A feedback mechanism containing CSI is required in order for the precoder to pre-distort the signals appropriately [6]. Precoding in an MMF system would require a Mach-Zehner modulator at the transmitter, versus a simple on-off scheme used in classic optical systems. Such a replacement, however, is a very inexpensive option compared to adopting coherent detection at the receiver [9]. Additionally, precoding also would improve performance during propagation and allows for proper coding to maximize channel performance. In this thesis, the concept of precoding is explored and applied to an MMF system with the intent of enabling medium distance transmission.

Table 1.1: A comparison of signal processing methods.

<b>Technique</b>	<b>Pros</b>	<b>Cons</b>
Receiver Equalization	CSI readily available	Requires expensive coherent detection
Launching of Specific Modes	No transmitter or receiver processing required	Does not eliminate ISI
Precoding	Costly coherent detection avoided	CSI not readily available

## 1.4 Thesis Outline

The rest of the thesis is organized as follows. Chapter 2 details the analytical MMF model utilized for our research, including an in-depth study of the root causes of modal dispersion and system degradation in the channel. In Chapter 3, we present an overview of an MMF system from transmitter to receiver. Chapter 4 discusses the theory behind the creation of the precoder and simulation results when applied to an MMF that experiences various levels of modal coupling. Chapter 5 presents conclusions with recommendations for future work.

## 1.5 Chapter Summary

In Chapter 1, we discussed the optical fiber capacity crunch problem, along with the dramatic rise in data consumption. As single-mode fiber capacity is reaching its limit, we have established that MMFs hold great potential to increase data throughput over long distances. However, modal dispersion in MMFs is a very present hindrance to enhancing capacity. After discussing both receiver processing and launching of other modes, we introduce precoding as

unchartered territory to increase MMF capacity, and is the focus of this thesis. Finally, we concluded Chapter 1 with an outline of the rest of the project.

## Chapter 2-System Model

In this chapter, we describe the model used to design and simulate an enhanced MMF communication system. The block diagram of the proposed system is provided in Figure 2.1. For this thesis, the system begins by generating 3 input signals and converting each information signal into an optical component. The subsequent optical signals arise from a power split from a signal optical source. Each signal is then modulated via a Mach-Zehnder modulator (MZM) to give the signal the necessary magnitude and phase components determined from the precoder. Each signal is then multiplexed spatially, and propagated through the MMF. At the receiver, the signals are de-multiplexed and detected using square-law direct detection [6]. For each coherence interval, training sequences are used to determine the proper coefficients of the precoder, as described in Chapter 4.

It is beyond the scope of this thesis to pay any particular attention to the most recent technology or capture every limiting detail of the optical hardware. Hence, several approximations and assumptions have been made to simplify the computation required. Several scenarios were examined where the receiver was assumed to be noiseless or introduced additive white Gaussian noise to the system.

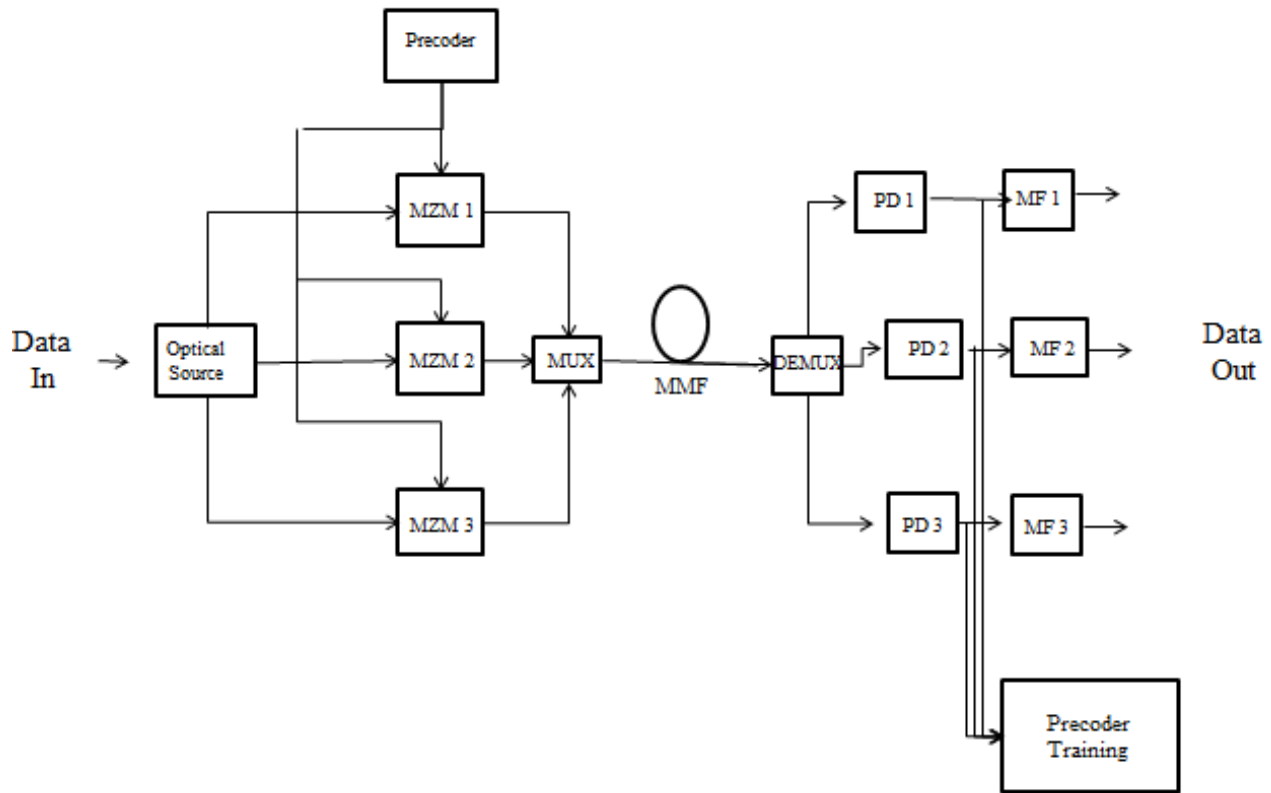


Figure 2.1: MMF system model.

## 2.1 Transmitter

There exist two methods of modulating an input signal onto an optical wave. One technique is external modulation, where the light source itself is modulated and subsequently applied to the input signal. An alternate method, known as direct modulation, supplies modulated electric current to the laser, which therefore modulates the light itself. In many optical systems, on-off keying is utilized, where high and low bits are designated by turning the laser on or off respectively. In this thesis, each mode uses the same laser and, ergo, each signal has the same phase. Transmitting from the laser allows the phase at the receiver to be more predictable. Should each mode be transmitted with a different laser, the phases would all differ from each other, causing the signals from the very beginning to be noncoherent.

For this simulation, non-return to zero (RZ) pulses were used, where each bit occupies the entire bit duration, which is the inverse of the system bit rate [2]. Super Gaussian pulse shaping was applied for this model [6]. The impulse response of a super Gaussian pulse shaping filter is described by (3.1) below, where the parameters  $P$ ,  $t_0$ , and  $m$  signify the peak transmitted power, pulse width, and filter order respectively [2]. Equation (2.1) is considered to be a super Gaussian filter when  $m > 1$ . Additionally, the impulse response of the super Gaussian filter used in this work is shown in Figure 2.2, with the key difference from a typical Gaussian filter being that the top of the impulse response is much flatter depending upon the choice of  $m$ .

$$p(t) = P e^{-\left(\frac{t}{t_0}\right)^{2m}} \quad (2.1)$$

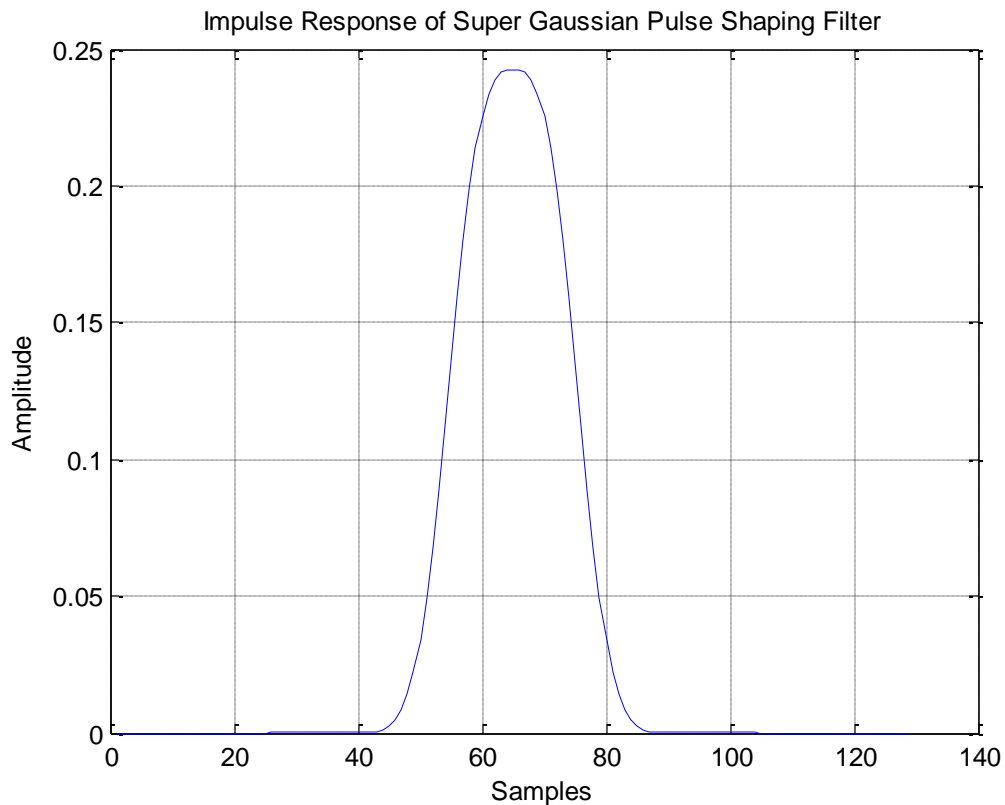


Figure 2.2: The super Gaussian pulse shaped filter used in this work, where  $m = 3$ .

Each bit stream is encoded onto a spatial mode and multiplexed into the precoder of the system, which is discussed in the following section [6]. The bit rate for each simulation was 1 Gbit/s, consistent with [6].

## **2.2 Precoder**

As mentioned in the previous section, a precoder is applied to each of the optical signals prior to multiplexing and propagation through the MMF. Precoding is a signal processing technique that removes negative channel effects before propagating through a communication channel. This method, in addition to correcting for channel effects, yields many benefits for communication systems overall, including the alleviation of computational complexity at the receiver and the creation of a code that maximizes system performance. In particular, the introduction of a precoder benefits fiber optic systems greatly by eliminating the need for computationally heavy coherent detection at the receiver, which retains phase information. Instead, the design and installation of a precoder requires an inexpensive Mach-Zehnder modulator, a device used to alter the amplitude and phase of an optical wave [2]. The proper precoding weights are determined at the receiver and sent back to the transmitter once per coherence interval, a feasible option since the coherence interval for optical systems is within the millisecond range [17]. The process used to determine the proper weights for the frequency flat and selective cases are provided in Chapter 4.

## **2.3 Multimode Optical Fiber**

The simulated MMF contained three weakly guided modes, which are commonly referred to as linearly polarized or LP modes. The strength for the fundamental and secondary modes are

described by (2.2) and (2.3) respectively below, with  $r$  representing the distance from the fiber center,  $\varphi$  signifying the rotation angle, and  $\xi$  denoting the mode field radius [6].

$$E_{01}(r, \varphi) = \frac{1}{\sqrt{\pi}} e^{-\frac{r^2}{2\xi^2}} \quad (2.2)$$

$$E_{11}(r, \varphi) = \sqrt{\frac{2}{\pi}} r e^{-\frac{r^2}{2\xi^2}} \begin{cases} \sin(\varphi) \\ \cos(\varphi) \end{cases} \quad (2.3)$$

The MMF length simulated was 50 km long. Several MMF models exist, but do not include modal dispersive effects or do not account for such effects properly, a point that is discussed in further detail in Section 3.3. The model described in Chapter 3, which is drawn from Juarez et al in [6], accurately captures MMF coupling and ISI behavior, and hence was used for this thesis. The MMF considered was loselss and did not account for the effects of attenuation. The center wavelength used in this model was 1.55  $\mu\text{m}$ . As will be discussed in greater detail in Section 3.2, the amount of coupling present within the MMF is dictated by the amount of mismatching between two simulated sections of the fiber, known as the splice mismatch ratio. The amount of mismatching was 0.01 and 0.05, and yielded coupling losses between approximately 0 dB and -14 dB for each of the three modes. A low splice mismatch of 0.01 as opposed to a splice mismatch of 0 was introduced to avoid computational issues, specifically with dividing by zero. The random rotation angle between two MMF segments and random phase variation parameter, as discussed in Section 3.2 as well, were a random values chosen between 0 and  $\frac{\pi}{4}$ , and 0 and  $2\pi$  respectively, also consistent with [6].

## 2.4 Receiver

First, de-multiplexing of the signals is mimicked at the receiver through a concept known as detection filtering, where each output vector is scalar multiplied by a detection vector,  $d$ . For

instance, the fundamental mode is extracted by multiplying the output vector by  $d = (1\ 0\ 0)^T$ , and the concept is extended to separate the secondary modes[6]. Photodiodes then perform direct detection (DD) on each signal, which outputs the power envelope of each optical signal. DD is a noncoherent detection technique and eliminates phase information from the received signals. Matched filtering is then applied to each signal, whose impulse responses are the time reversed super Gaussians used for pulse shaping. Downsampling is then applied to retain the original digital sequence transmitted. Typical lightwave systems with DD employ thresholding to make bit decisions, where a sample that is over or under a certain threshold is denoted as ‘1’ or ‘0’ respectively. Several simulations account for the effects of noise incurred during signal reception. Noise was modeled as additive white Gaussian noise (AWGN) to account for distortion from the electronics, such as shot noise, etc. AWGN was added with regards to the power of a single bit transmitted through the MMF, which was determined to be 0 dB constant for all signals.

## 2.5 System Performance Evaluation

There is no consensus on a performance criterion for lightwave systems. Several methods exist and are utilized depending on the parameter examined in the system. One of the most commonly used techniques is to measure the bit error rate (BER), a quantity that describes the fraction of incorrectly decoded bits incurred during propagation. The BER was utilized to measure the effectiveness of the precoders, in addition to measuring the effects of ISI and modal coupling present in the MMF. With no ISI present, the BER of an NRZ-OOK modulation scheme is given by (2.4) below, where  $erfc$  represents the complimentary error function.

$$P_b = \frac{1}{2}erfc\left(\frac{1}{2\sqrt{2}}\sqrt{SNR}\right) \quad (2.4)$$

Additionally, the performance of the MMF was gauged using the eye opening penalty (EOP), a quantity that effectively measures the ratio of how much ISI is incurred after propagation. The EOP is computed using (2.5) below, where  $EO_{BTB}$  and  $EO$  represent the back-to-back eye opening and the difference between the minimum value of a ‘1’ bit and maximum value of a ‘0’ bit [6].

$$EOP = 10\log\left(\frac{EO_{BTB}}{EO}\right) \quad (2.5)$$

A high EOP value is indicative of a small eye opening of the eye diagram for the system, meaning that ISI is very much present within the communication channel. Conversely, a low EOP value signifies a large eye opening of the “eye” and, ergo, very little ISI is present within the system [6].

## 2.6 Chapter Summary

In Chapter 2, we discussed the system model used to simulate MMF behavior. Specific parameters for the transmitter and receiver, such as the pulse shape and type of detection used, are presented and discussed. A precoding unit is introduced to alleviate channel dispersive effects prior to signal propagation, which introduces many benefits to the system overall, such as reduced computational complexity. Finally, the performance criterion, BER, used to evaluate the effectiveness of the precoding unit was detailed.

## Chapter 3-Channel Model

In this chapter, we describe the mathematical model used in MMF simulations and analysis for this thesis. In [6], Juarez et al develop an analytical method to create a channel matrix, denoted as  $T(\omega)$ , to characterize the frequency selective characteristics of an MMF when utilized for long-haul applications. As opposed to other models, which will be discussed later in the chapter, [6] simulates MMF behavior by first dividing the fiber in  $M$  sections that are of equal length, shown in Figure 3.1 below. In this thesis, the 50 km fiber was divided into 500 sections that are each 100 m long in order to simulate the effects of an actual fiber appropriately.

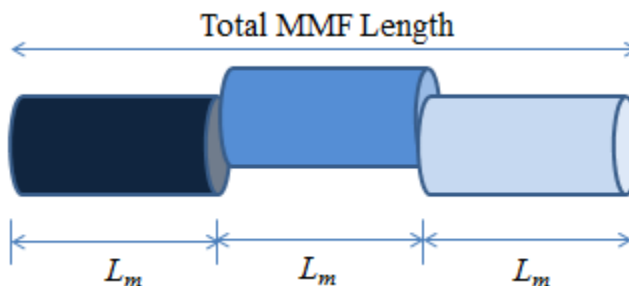


Figure 3.1: An MMF divided into sections of equal length,  $L_m$  [6].

Subsequently, the coupling and propagation delay characteristics, which are signified by  $K_m$  and  $M_m(\omega)$  respectively for the  $m$ 'th section, are computed for each section of the fiber. The transmission matrix for each fiber section,  $T_m(\omega)$ , is then the product of the aforementioned matrices. The channel propagation matrix of the MMF as a whole is then computed mathematically as the product of each transmission matrix of the fiber sections, which is described by (3.1) below [6].

$$T(\omega) = \prod_{m=1}^M T_m(\omega) = \prod_{m=1}^M M_m(\omega)K_m \quad (3.1)$$

A proper estimation of the amount of coupling and propagation delay experienced between modes is key to achieving an accurate description of the MMF channel. Each section

channel matrix is also made up of an ideal propagation matrix, signified by  $M_m(\omega)$ , which describes the amount of delay taken on by each mode in that particular section. The differential delay, and ultimately the amount of ISI incurred during propagation in an MMF section, is dictated by  $M_m(\omega)$  and is discussed in greater detail in Section 3.1. The coupling matrix, denoted as  $K_m$ , models the amount of power exchanged between each mode of a fiber, and is ultimately a function of misalignment between fiber sections, as discussed further in Section 3.2.

### 3.1 Ideal Propagation Modeling

The ideal propagation matrix, denoted in (3.1) as  $M_m(\omega)$ , describes the amount of propagation delay, which we will show is a sign of ISI and pulse broadening, taken on by each mode in a particular MMF section. As noted in classic signals and system theory, the delays incurred by each mode are modeled by a complex exponential in the frequency domain as a function of frequency,  $\omega$ .  $M_m(\omega)$  is a diagonal matrix in order to simulate purely delays, and is thus described by (3.2) below [6].

$$M_m(\omega) = \begin{pmatrix} 1 & 0 & \dots & 0 \\ 0 & e^{-j(\Delta\phi_1 + \zeta_{1,m})} & 0 & \vdots \\ \vdots & 0 & \ddots & 0 \\ 0 & \dots & 0 & e^{-j(\Delta\phi_l + \zeta_{l,m})} \end{pmatrix} \quad (3.2)$$

The amount of delay in (3.2) is ultimately a function of fiber geometry and is the root cause of ISI and pulse broadening incurred during propagation through a given MMF section. Fluctuations in strain or temperature of the fiber are described by a random phase parameter denoted by  $\zeta_{l,m}$ . The parameter  $\Delta\phi_l$  featured in the exponents of (3.2) are determined as a combination of the differential propagation and group delays, signified by  $\Delta\beta_l$  and  $\Delta\tau_l$

respectively, in addition to the MMF section length, and the frequency. Mathematically,  $\Delta\phi_i$  is determined by (3.3).

$$\Delta\phi_i = (\Delta\beta_i + \Delta\tau_i\omega)L_m \quad (3.3)$$

The propagation constant,  $\beta_i$ , of the  $i$ 'th fiber mode dictates the change of the wave amplitude during propagation through the fiber [2]. When LP or weakly guided modes are assumed, meaning that the refractive indices of the core,  $\eta_{co}$ , and the cladding,  $\eta_{cl}$ , are nearly equivalent, the propagation constant is determined by (3.4) below, where  $q$  and  $l$  represent the radial and circumferential orders of the mode respectively. The relative index difference is computed by  $\Delta = (\eta_{co} - \eta_{cl})/\eta_{co}$  and  $r_0$  signifies the diameter of the MMF core [6].

$$\beta_{q,l} = \eta_{co}k_0\sqrt{1 - \frac{2\sqrt{2\Delta}}{\eta_{co}k_0r_0}(2q + 2l + 1)} \quad (3.4)$$

The value of the propagation constant lies within a certain range dictated by the refractive indices of the core and cladding and the free space wave number, a function of the wavelength and calculated by  $k_0 = 2\pi/\lambda$ . The range for the propagation constant of the  $i$ 'th mode is shown in (3.5) below [10].

$$\eta_{cl}k_0 < \beta_j \leq \eta_{co}k_0 \quad (3.5)$$

The exponential delays described in (3.2) and (3.3) are, however, partially dependent upon the differential propagation constants,  $\Delta\beta_i$ , a quantity that is quite informative regarding the amount of coupling between modes. The differential propagation constant describes the difference between the complex phase changes of two modes. A large  $\Delta\beta_i$  value indicates that the modes under investigation are traveling at drastically different speeds. In turn, the two modes travel together very briefly and, therefore, have a small opportunity to exchange power, which results in low levels of ISI. Alternatively, a small differential propagation constant implies that the two modes are travelling at the same speed. Ergo, the modes have a large period

of time to exchange power, resulting in large amounts of ISI and signal distortion [11]. Should the propagation constants of each mode be unavailable, the differential propagation constant can be estimated by (3.6) below [12].

$$\Delta\beta = \frac{\sqrt{2\Delta}}{r_0} \quad (3.6)$$

Additionally, the delays in (3.2) are also dependent upon the differential group delay relative to the fundamental mode of the fiber. The group delay constant,  $\tau$ , provides the required propagation time for a given mode. A key characteristic of group delay is that it is directly scaled with fiber length, so a longer fiber will have a longer propagation time [2]. The group delay for a linearly polarized (LP) mode is determined by (3.7) below [6].

$$\tau_{q,l} = \frac{N_1}{c} \left( 1 + \Delta \left( \frac{2q+l+1}{\eta_{cl} k_0 r_0} \right)^2 \right) \quad (3.7)$$

The differential group delay,  $\Delta\tau_l$ , is the measure of the propagation delay between modes in a given MMF section. The difference in propagation speeds causes pulse broadening at the photodetector and is also seen as a measure of ISI [11]. The differential group delay can be estimated by (3.8) below, where  $N_1$ ,  $c$ ,  $M$  and  $\delta$  are the group index, the speed of light, the number of modes respectively, and relative delay spread [13].

$$\Delta\tau = \frac{N_1\delta}{cM} \quad (3.8)$$

## 3.2 Modal Coupling Modeling

The coupling matrix, represented by  $K_m$  in (1), describes how perturbations in the fiber effect propagation, particularly with regards to power transfer between modes [13].

Imperfections that exist in an MMF are accounted for by simulating the MMF as being multiple segments spliced together, similar to the concept in Figure 3.1. When splicing two actual fibers

together, it is impossible to align sections with absolute precision and mismatches are bound to occur, resulting in additional distortion upon signals propagating in an MMF [13]. The model developed in [6] uses the concept of misalignment between MMF sections to describe for disturbances in the MMF. Splice mismatching is depicted in Figure 3.2 below.

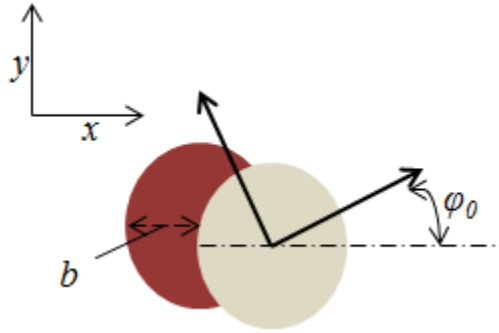


Figure 3.2: Misalignment between MMF sections with regards to radial offset and rotation angle [6].

The coupling matrix can be calculated via (3.9) below, where  $i$  and  $j$  are not equivalent and represent different modes, where  $\xi$  represents the mode field radius [6].

$$K_m = \frac{1}{\xi^2} \iint_{-\infty}^{\infty} E_{i,m}(x, y) E_{j,m+1}^*(x', y') dx dy \quad (3.9)$$

When (3.9) is expanded, given the proper assumptions and mode information,  $K_m$  is a function of the radial offset and random rotation angle, denoted as  $b$  and  $\varphi_0$  in Figure 3.2, between two MMF sections. The radial offset is of particular interest due to its strong impact upon the amount of coupling present in the channel. Large radial offset between two MMF sections will create a great amount of coupling and, likewise, a small radial offset will result in low amounts of coupling. Ultimately, the coupling matrix induces a splice loss,  $\alpha$ , that reveals how much power is lost as a result of splice mismatching [6].

### 3.3 MMF Channel Analysis

The ISI and dispersion effects upon the MMF were examined via simulation using the model described throughout this chapter under two different modal coupling cases. The first situation investigated was the MMF without any modal coupling, meaning that the fiber sections were spliced perfectly in alignment with each other. The splice mismatch in this instance was 0.01 and induces a coupling loss of nearly 0 dB for the fundamental mode and roughly -7 dB for the secondary modes. The magnitude spectrum, phase spectrum normalized to  $\pi$ , and impulse responses for the MMF with little coupling are shown in Figures 3.3, 3.4, and 3.5 respectively.

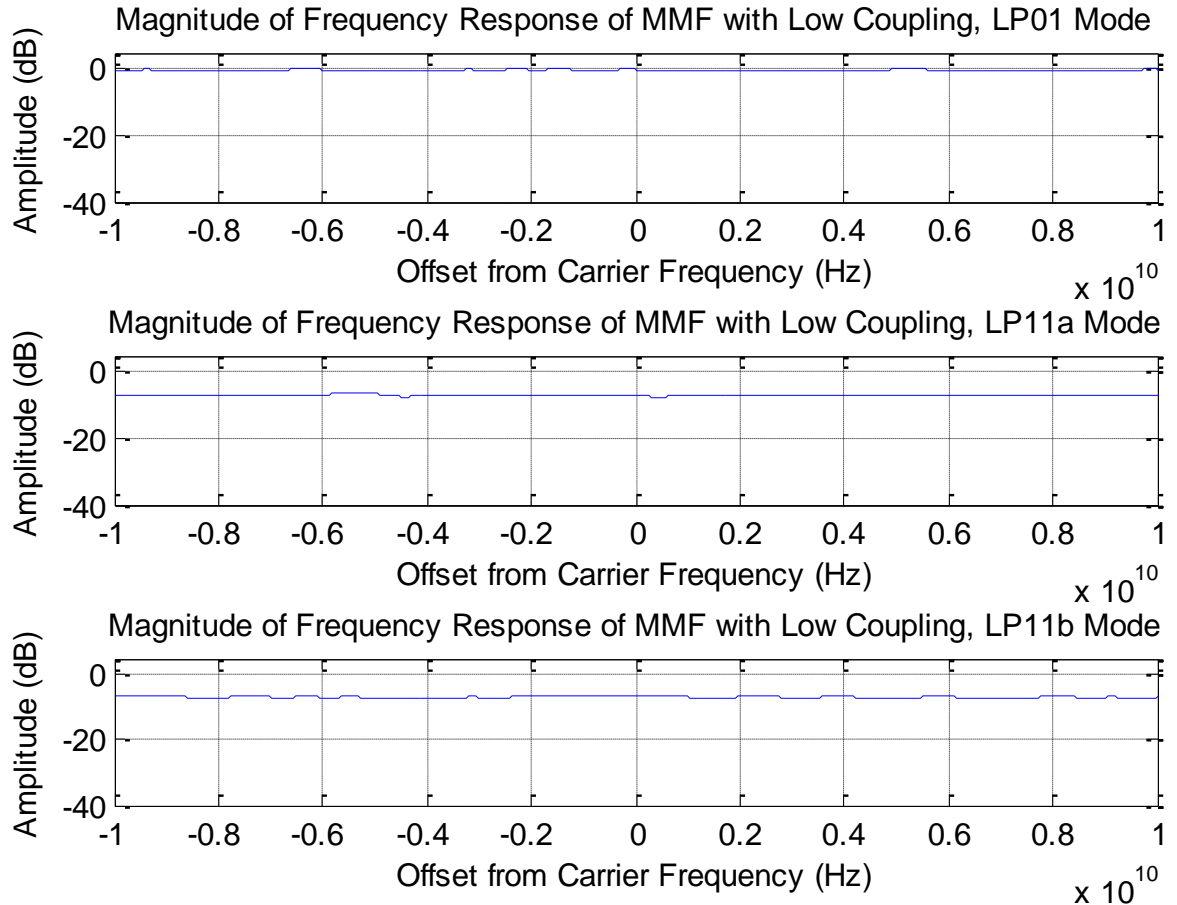


Figure 3.3: Magnitude spectra for each mode of MMF with low coupling.

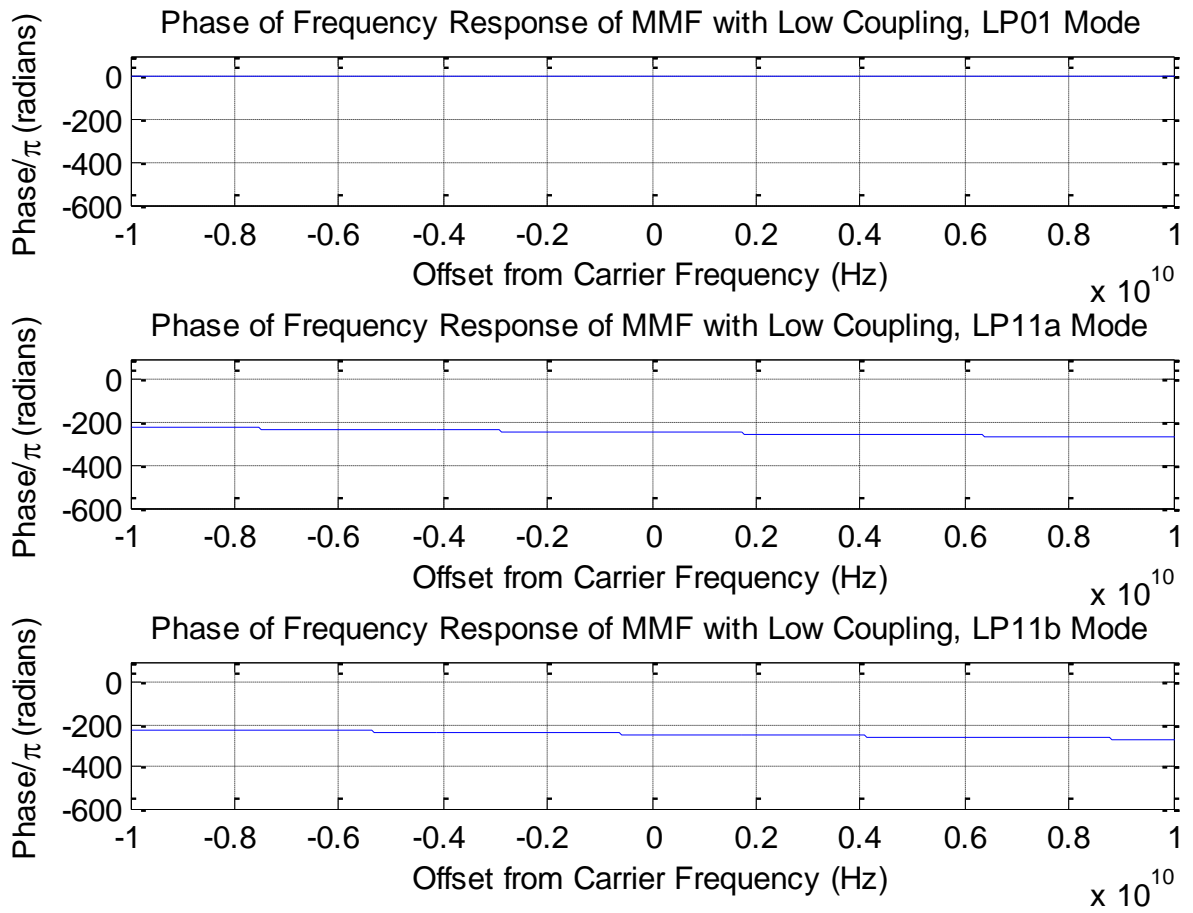


Figure 3.4: Phase spectra for each mode of MMF with little coupling.

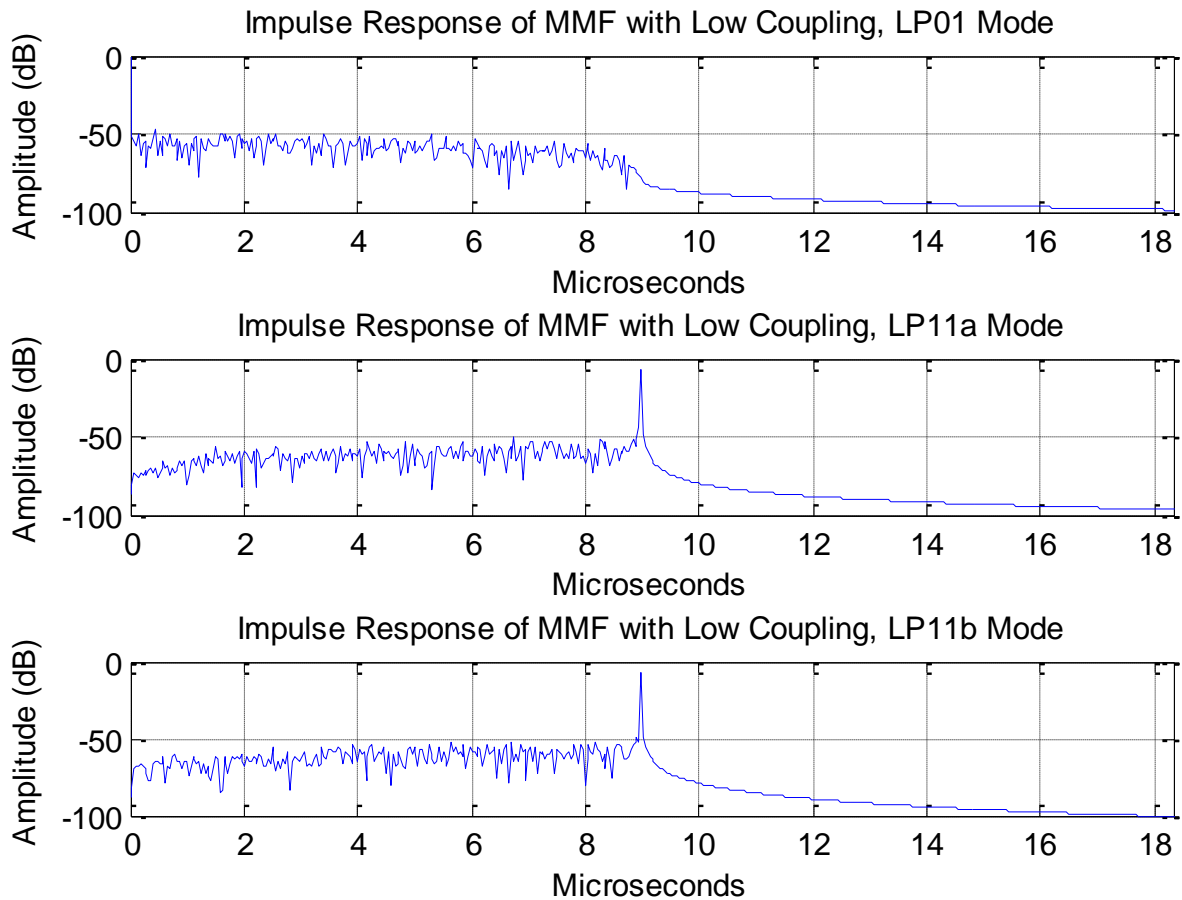


Figure 3.5: Impulse response for each mode of MMF with little coupling.

When little modal coupling exists, the frequency responses for each mode in the MMF are relatively frequency flat, as illustrated in Figure 3.3, and therefore can be generally described by a single channel matrix for all frequencies. The magnitude of the frequency responses for the secondary modes shows some fading, caused primarily by modal mixing with each other since the two modes share a propagation constant. The coherence bandwidth for each LP01, LP11a, and LP11b modes is approximately 220 Hz, 600 Hz, and 150 Hz respectively, which are all substantially below the bandwidth of the MMF and indicates that each mode experiences dispersion.

The phase spectra in Figure 3.4 further support how much dispersion is present within the MMF, particularly with regards to the secondary modes. For the LP01 mode, the phase spectrum is relatively constant and does not vary considerably. However, the LP11a and LP11b modes have linear phases with a fairly steep slope, due to the delay compared with the LP01 mode.

The system characteristics were also examined in the case where high modal coupling was present, meaning that the fiber sections were severely misaligned during splicing. The splice mismatch parameter was set to 0.05, considered high when the sections are shorter than in [6], which induces coupling losses of roughly -3.5 dB for the fundamental mode and -14 dB for the secondary modes. The magnitude spectrum, phase spectrum normalized to  $\pi$ , and impulse responses for the MMF with high coupling are shown in Figures 3.6, 3.7, and 3.8 respectively.

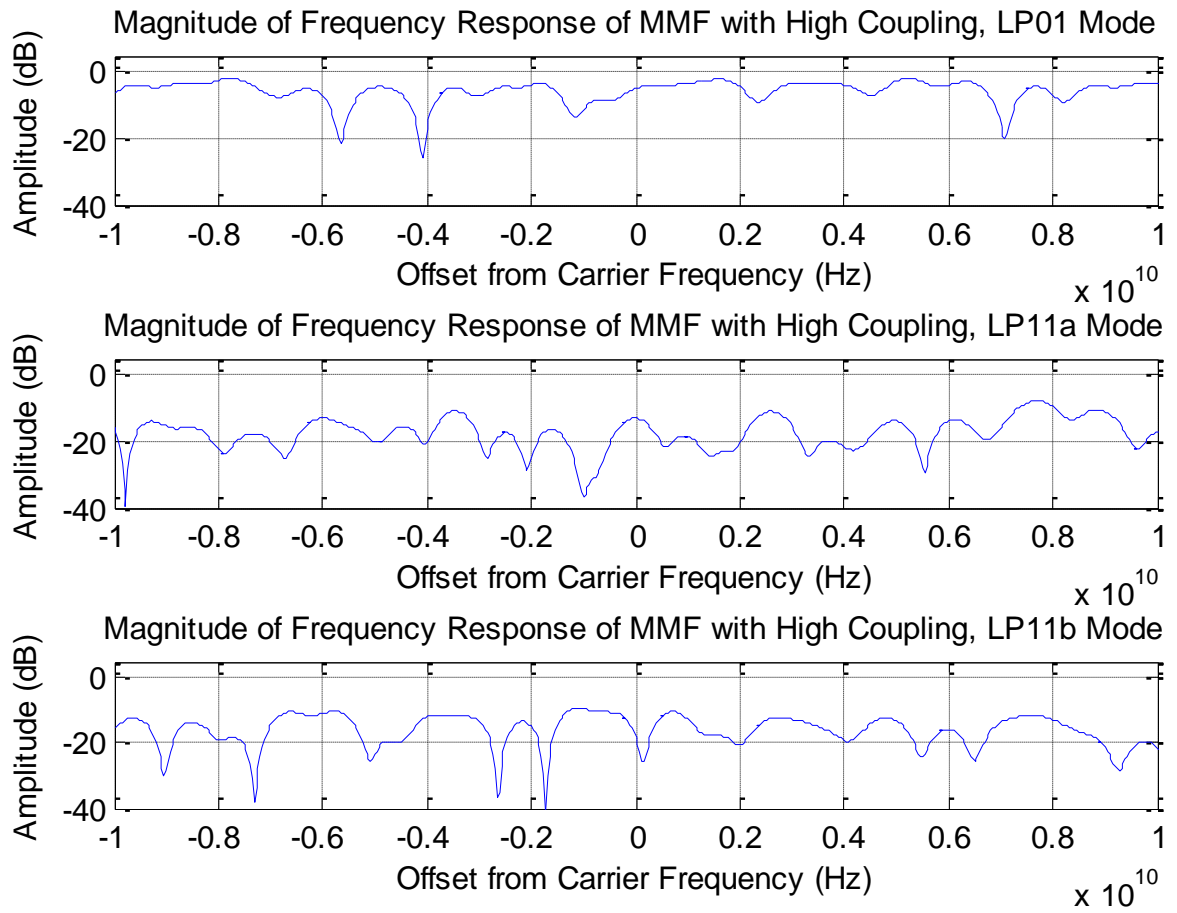


Figure 3.6: Magnitude spectra for each mode of MMF with high coupling.

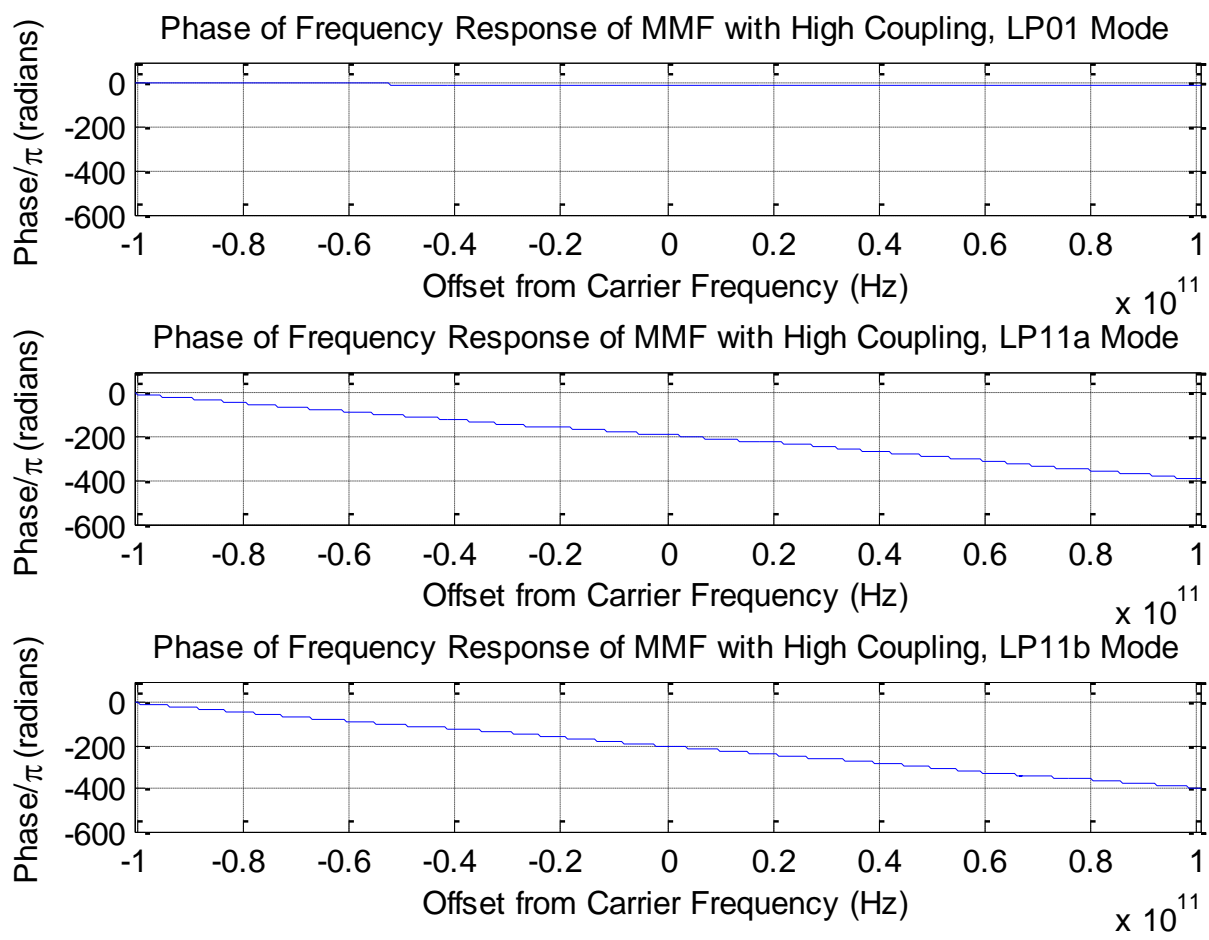


Figure 3.7: Phase spectra for each mode of MMF with high coupling.

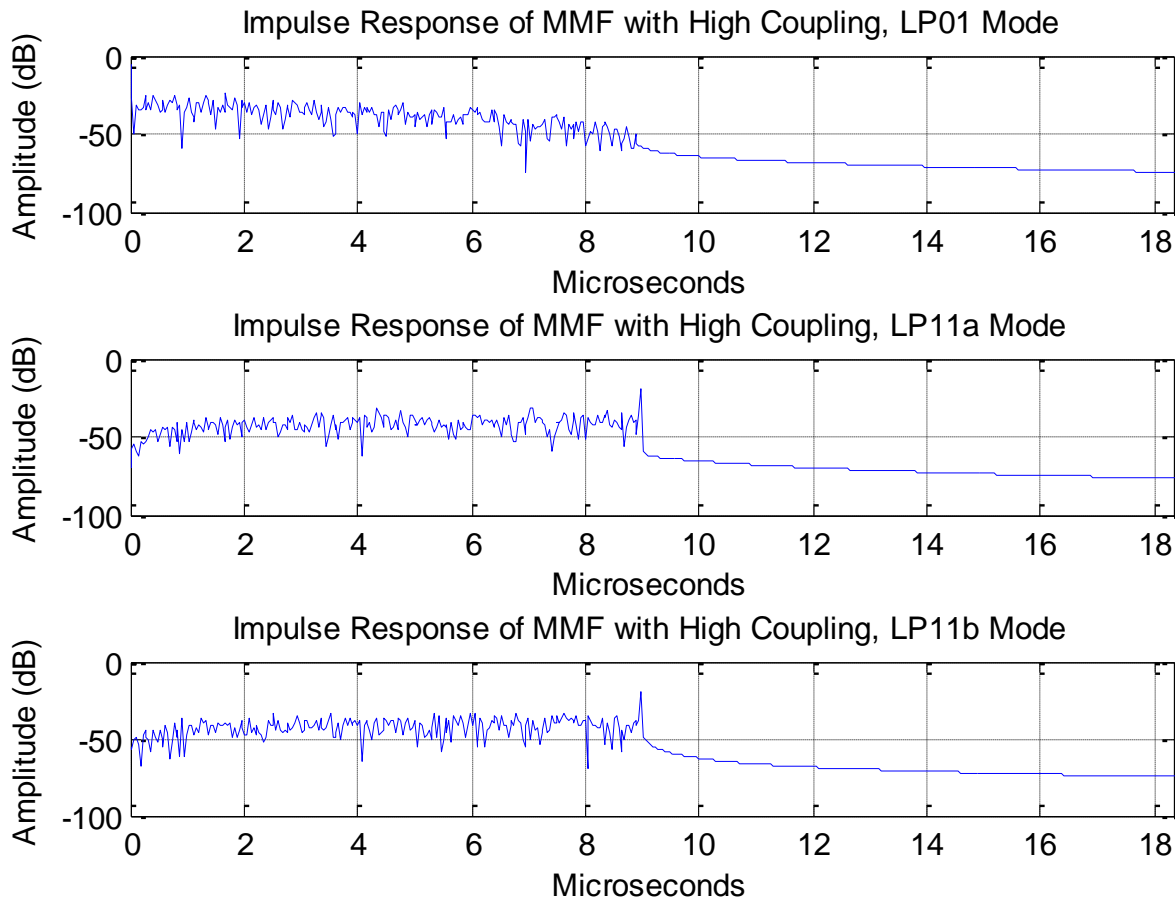


Figure 3.8: Impulse response for each mode of MMF with high coupling.

As opposed to the no coupling case, the frequency responses of each mode in the highly coupled MMF in Figure 3.6 vary wildly with frequency, demonstrating clear frequency selective behavior for each of the three modes in the MMF. Furthermore, the phase spectra of the each propagating mode is linear with a steep slope, a clear sign of dispersion present within each mode. The impulse responses of each mode in Figure 3.8 additionally show several smaller spikes, which indicates that the channel contains dispersive and time spreading effects. Finally, the coherence bandwidth for each mode, which are 61 Hz, 102 Hz, and 76 Hz for the fundamental and two secondary modes respectively, are substantially below the computed bandwidth of the MMF, a clear sign of ISI that leads to high BERs for each mode.

Additionally, we can assess the amount of ISI incurred on the channel by critiquing the eye diagram of each mode under different amounts of coupling. The eye diagrams were examined for MMFs under the same low and high coupling amounts described previously, i.e. splice mismatches of 0.01 and 0.05 without noise present. The eye diagrams of each mode, computed after the photodetector, are shown in Figures 3.9 through 3.11 and Figures 3.12 through 3.14 for the low and high coupling cases respectively.

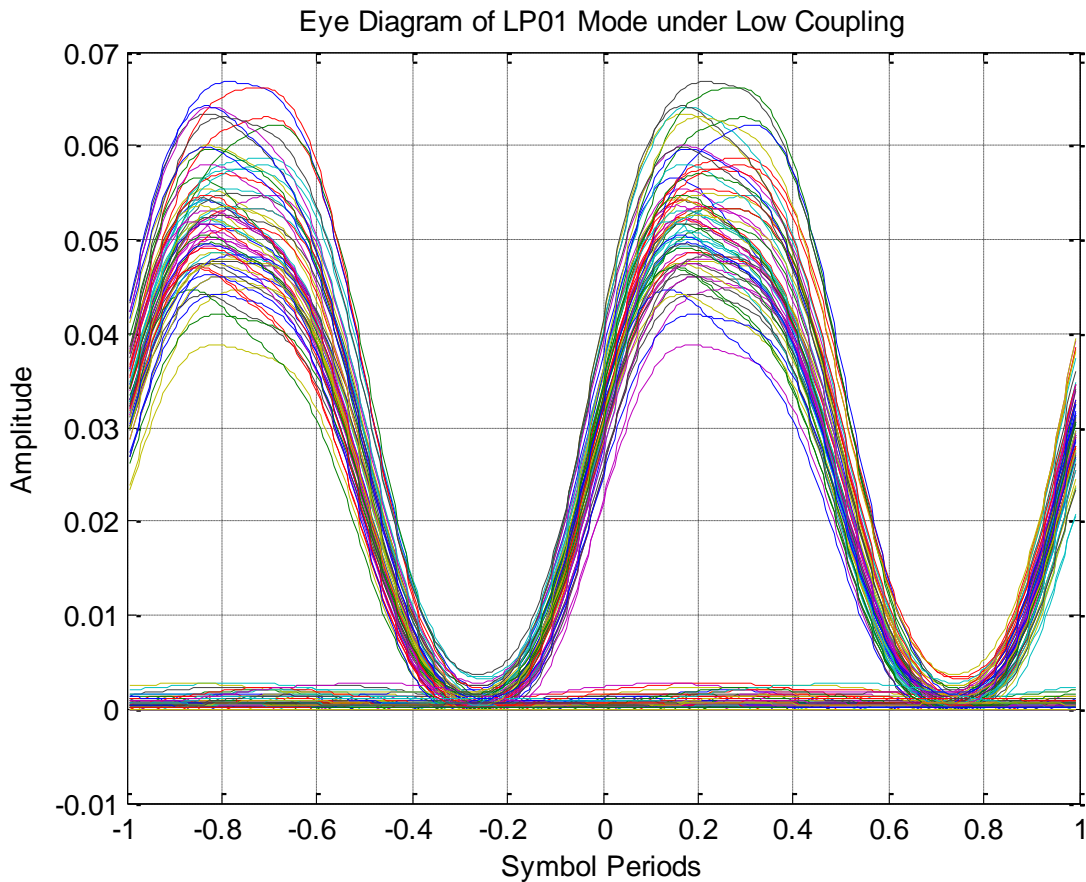


Figure 3.9: The eye diagram of the LP01 mode when the splice mismatch is 0.01.

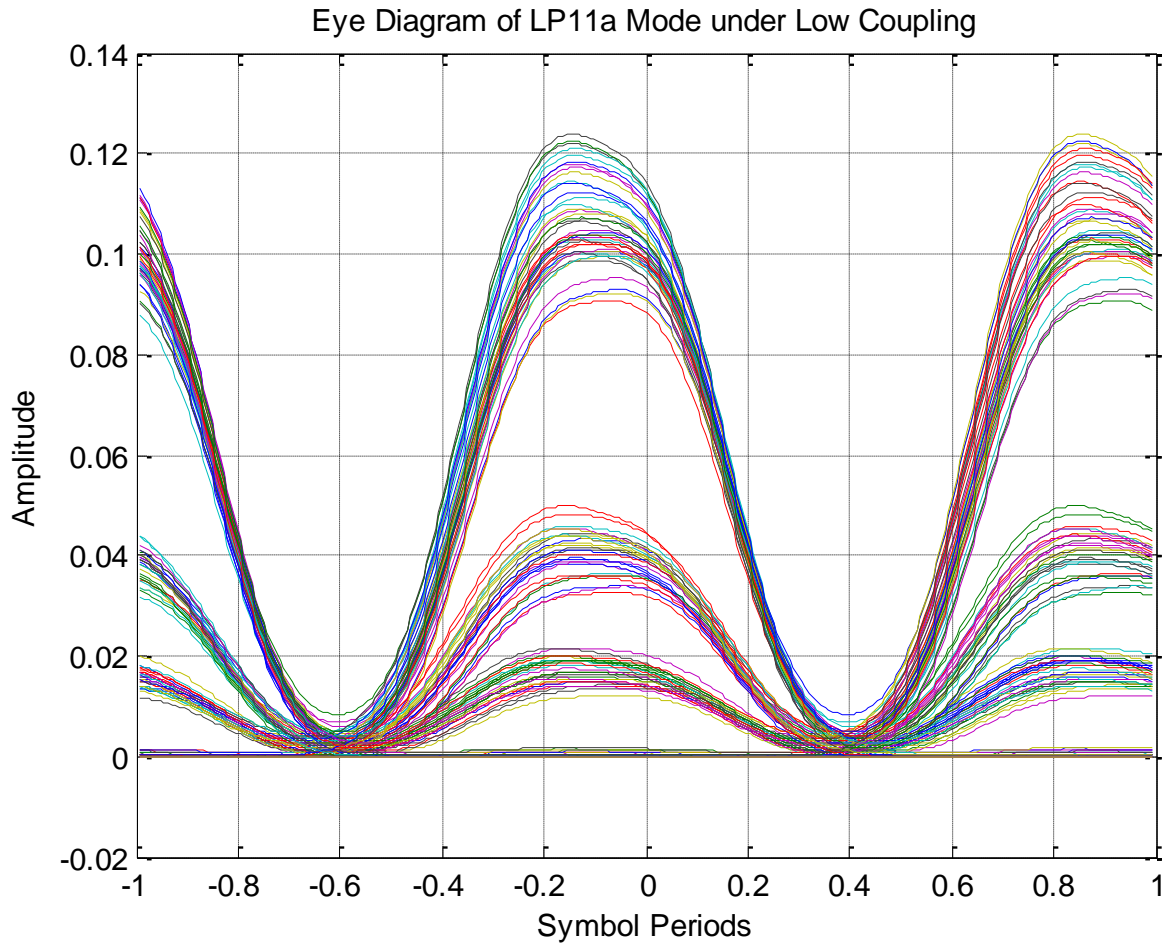


Figure 3.10: The eye diagram of the LP11a mode when the splice mismatch is 0.01.

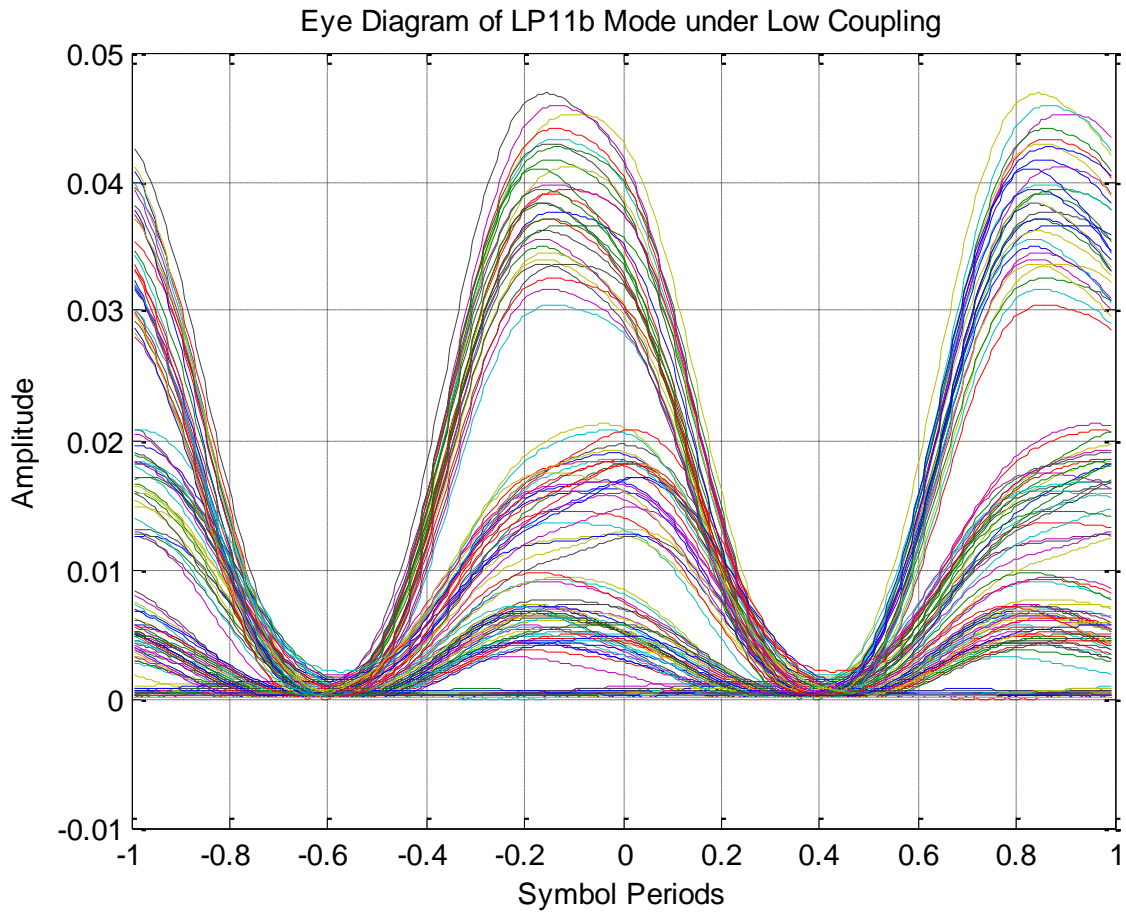


Figure 3.11: The eye diagram of the LP11a mode when the splice mismatch is 0.01.

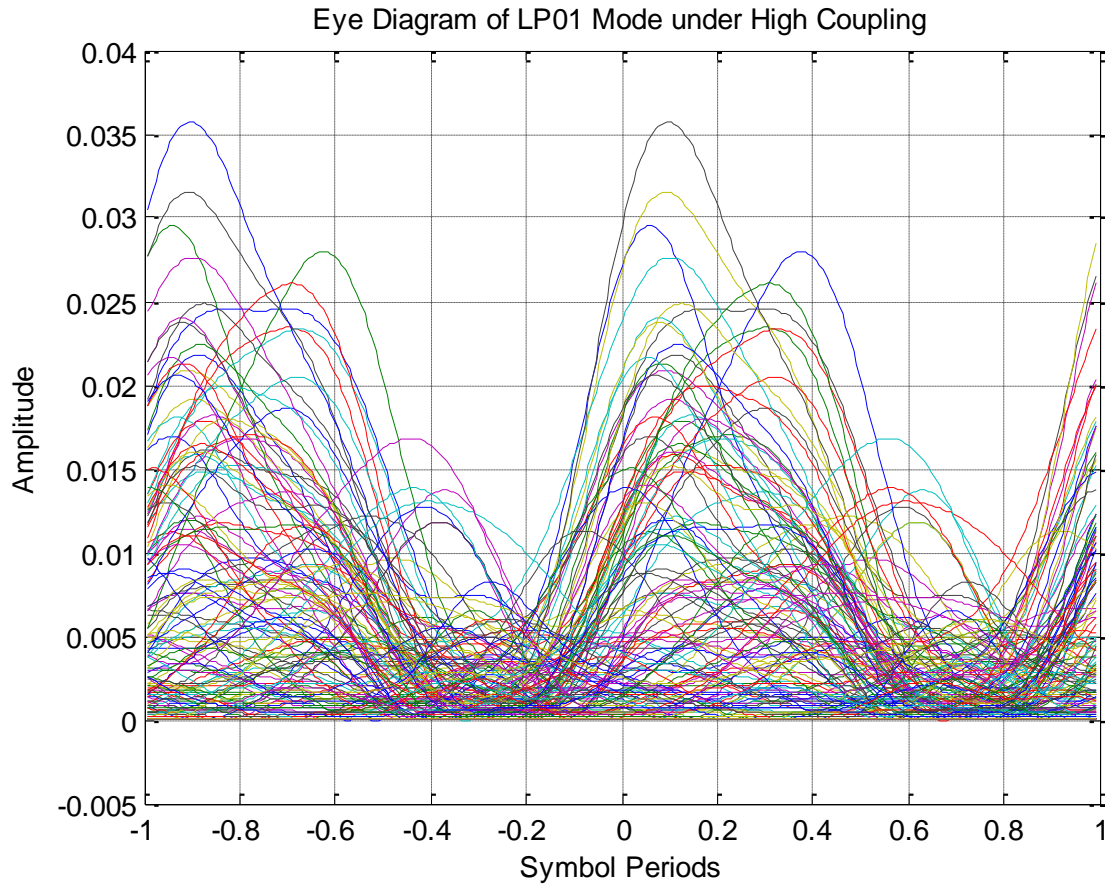


Figure 3.12: The eye diagram of LP01 mode when the splice mismatch is 0.05.

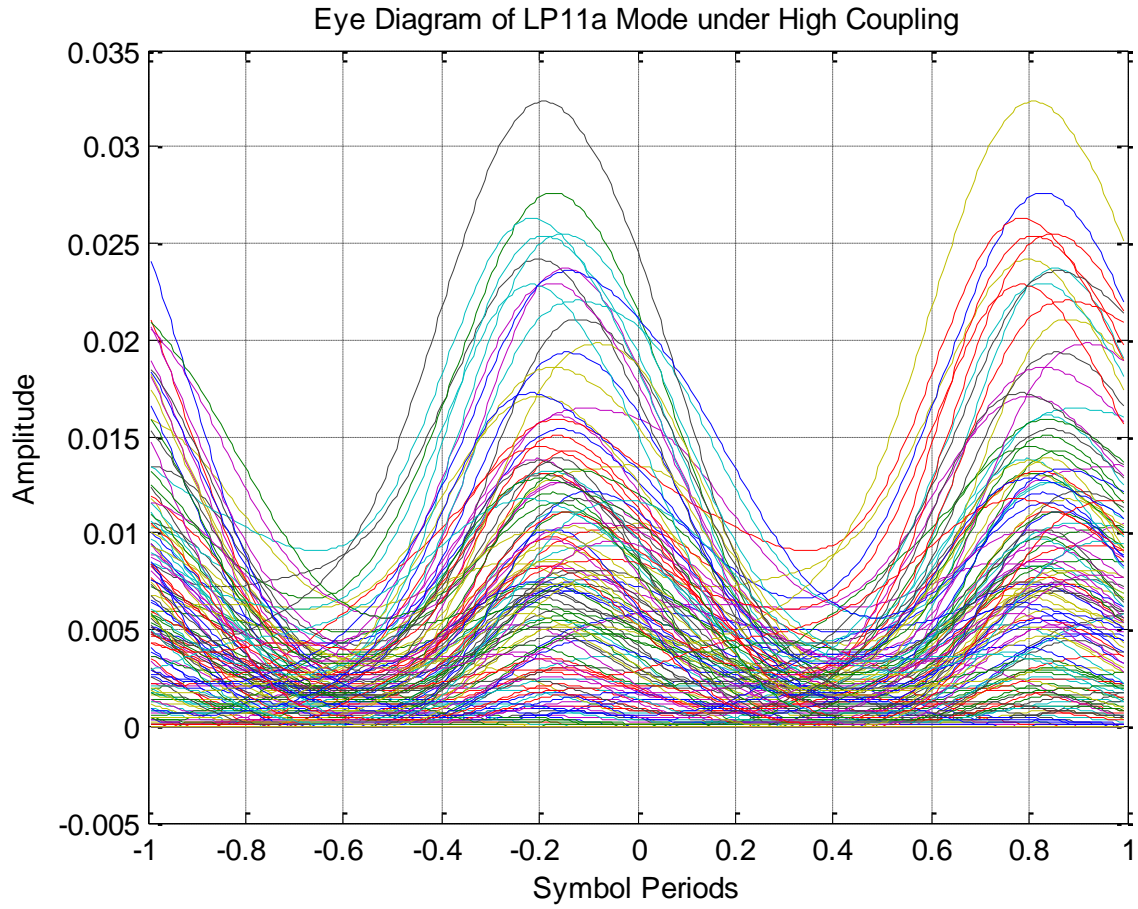


Figure 3.13: The eye diagram of LP11a mode when the splice mismatch is 0.05.

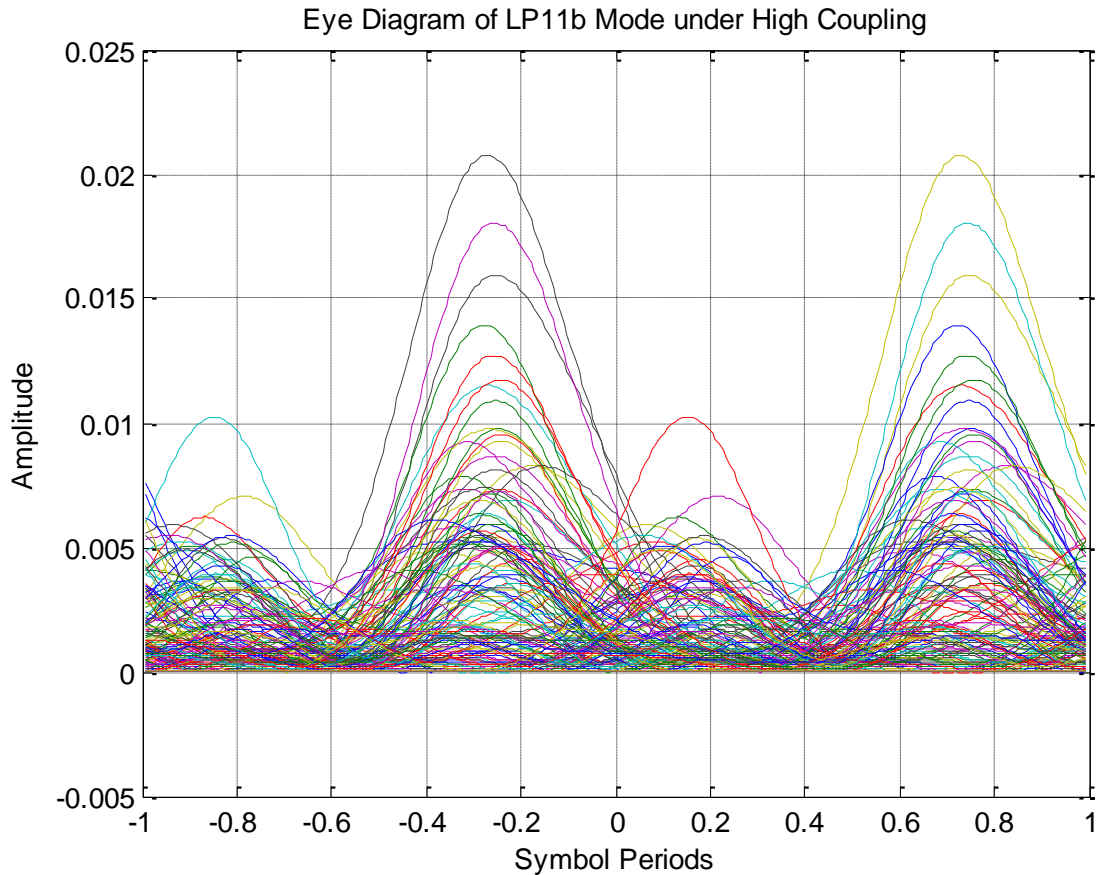
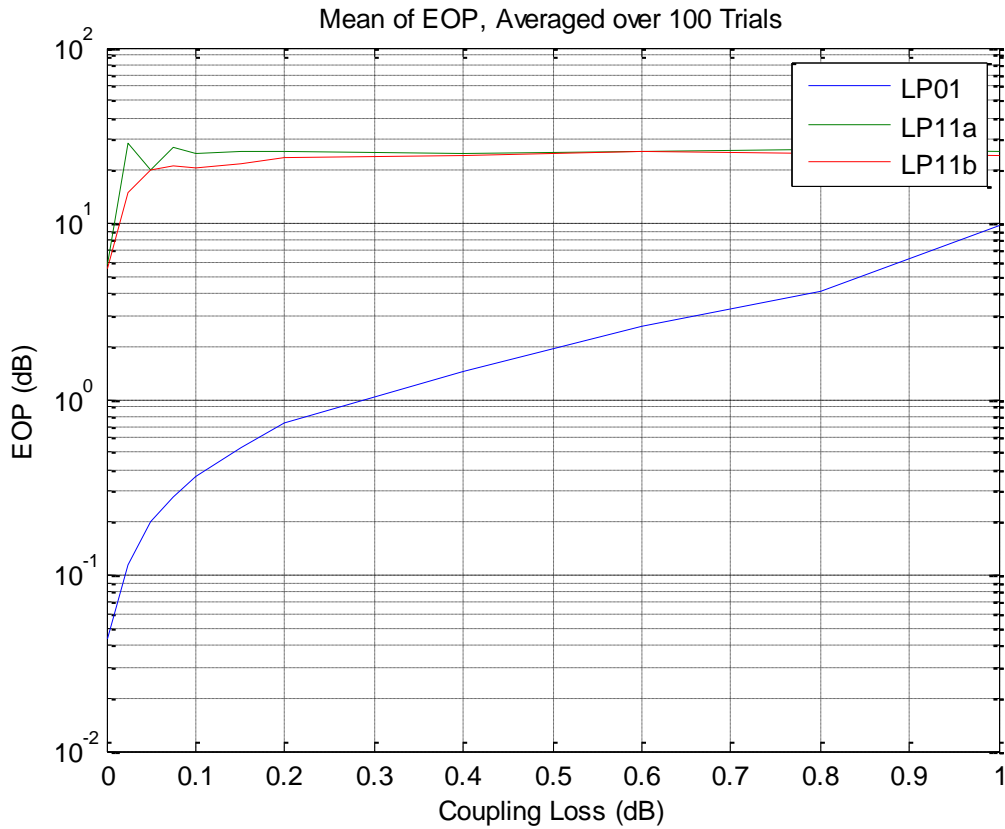


Figure 3.14: The eye diagram of LP11b mode when the splice mismatch is 0.05.

Figures 3.9 through 3.14 back up the claims made regarding the magnitude and phase spectra and the impulse responses for both the low and high coupling scenarios. In Figures 3.10 and 3.11, we note that the eye openings of the secondary modes are relatively small, a sign that ISI is present within the system. Conversely, the fundamental mode in Figure 3.9 has a very large eye opening and hardly suffers from ISI. When the coupling is extremely high in the case of Figures 3.12 through 3.14, the eyes of all three modes are completely shut and suffer severely from ISI and are unusable for transmission.

A final examination of the characteristics of the noiseless MMF involved the EOP as a function of the coupling loss induced by the MMF, which is a direct consequence of the amount of splice mismatching between modes. The EOP induced by various coupling losses is

illustrated in Figure 3.15 below and can be compared with Figure 5 in [6]. Figure 3.15 illustrates the EOP for an MMF simulated as being divided into 3 km sections and was used to validation the model with the original described in [6].



**Figure 3.15:** The EOP of each mode as a function of coupling loss.

Figure 3.15 highlights the performance of the MMF and is indicative of the ISI under low coupling conditions. The fundamental LP01 mode reacts as expected toward incurred coupling loss. When no coupling loss is present, the EOP of the first mode is low, suggesting that ISI is not a prominent issue. As coupling loss increases, however, we see in Figure 3.15 that ISI becomes a larger problem as the EOP rises as expected. In the case of the secondary LP11 modes, the EOP is more so a characteristic of the two modes rather than the coupling loss. Even in the absence of coupling, the EOP of both modes is relatively high and increases only slightly

when coupling is present. The secondary modes experience much higher EOP values due to the fact that they share a propagation constant and, thus, are highly coupled with each other.

### 3.4 Comparison to Other MMF Models

The model proposed by Juarez et al in [6] stands as a strong representation of MMF behavior, particularly in comparison to various models in existence. A key advantage to [6] is that the model can be used to analyze and propose solutions to MMF applications for long-distances, since modal dispersion and, hence, the frequency selective nature is taken into account. In many other models, modal dispersion is unaccounted to ease the situation, such as the model provided in [13]. Bikhazi et al approach MMF behavior for  $M$  photodetectors individually and compute each channel matrix, denoted as  $H^{(m)}$  for the  $m$ 'th photodetector via (3.10) below.

$$H^{(m)} = A^{(m)}\Gamma^{(m)}B \quad (3.10)$$

The channel matrix for each photodetector is a function of the coupling coefficients between modes,  $A^{(m)}$ ; the propagation before transmission into the MMF,  $\Gamma^{(m)}$ ; and the coupling between the  $n$ 'th bitstream and the  $q$ 'th mode,  $B$  [13]. The principal drawback to this model is that modal dispersion is unaccounted for and, thus, this model is only advantageous when considering short-haul applications. A similar approach to modeling MMFs is also seen in [5] and [15], where singular value decomposition is used to break down the channel matrix into simpler components. However, authors in [5] and [15] are unable to capture modal dispersive effects and model the characteristics of an MMF used in long-haul applications.

Alternatives exist that encompass modal dispersion when examining MMF behavior, but fail to capture modal dispersive effects properly. In [16], Arik et al study the modal dispersive

effects on individual MMF sections for a long-haul fiber, similar to that of [6], divided into a total of  $K$  sections. The modal dispersive component is a variant of singular value decomposition and is shown in (3.11) below, where  $k$  represents the  $k$ 'th fiber section.

$$M_{MD}(\omega) = \prod_{k=1}^K U^{(k)} \Sigma^{(k)} V^{(k)*} \quad (3.11)$$

Random coupling between modes is modeled by the unitary random matrices,  $U^{(k)}$  and  $V^{(k)*}$ , which are independently distributed over the  $k$ 'th MMF section. Additionally,  $\Sigma^{(k)}$  is a propagation matrix of uncoupled modes, a case where the modes are independent of each other and the channel therefore acts as frequency flat [16]. However, the model discussed in [16] is inaccurate due to the inaccurate presentation of modal dispersive effects in the fiber. As previously discussed in Section 3.2, modal coupling is not a random quantity and, rather, is deterministic in nature, as opposed to propagation delays in the fiber [13]. Hence, the model proposed in [16] is less than ideal.

### 3.5 Chapter Summary

In Chapter 3, we discussed characterization of MMF behavior through the model proposed by [6]. A proper description of MMF behavior begins by examining the propagation delay and modal coupling features of several, equidistant sections. The propagation delay is essentially a measure of ISI present in the system, particularly when considering the differential propagation constants contributing to the delays. Modal coupling is a result of splicing offset between fiber sections and results in high power exchanges between modes. Ultimately, the model presented in [6] is superior to alternative models due its capability to accurately capture the frequency selective nature when long-haul MMF applications are considered.

# Chapter 4-Precoder Construction and Performance

In this chapter, we describe the precoding method used to enhance system performance when the MMF experiences various levels of splice mismatch, and therefore various levels of coupling. Various methods exist to create a precoder, which include adaptive methods or a transmitting training bits to that exploit channel characteristics to create an appropriate precoder. We propose transmitting specific training bit sequences, such as  $(0\ 0\ 1)^T$ ,  $(0\ 1\ 0)^T$ , et cetera, several times per coherence interval to extract CSI. For fiber optic systems, a training scheme is practical since the coherence interval is relatively, within the millisecond range, when compared to wireless or other communication media. At the receiver, a filter update scheme is utilized to determine the appropriate precoder weights and subsequently feedback such values to the transmitter. The key concept is illustrated in Figure 4.1 below.

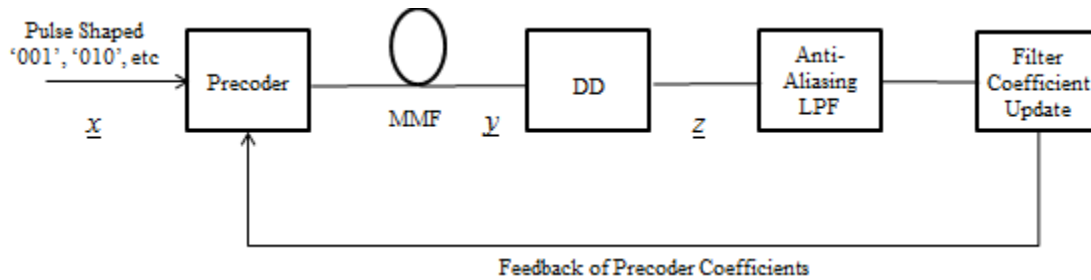


Figure 4.1: Feedback scheme used to pre-distort each bit stream into the MMF.

In Figure 4.1, we note that an anti-aliasing low pass Chebyshev type II filter is used in place of a matched filter. Matched filtering at the receiver can cause unintended alteration of the received signals to create the precoder and, therefore, produce less accurate estimates of the inverse channel matrix. Suppose we have the ideal scenario where the precoder is equal exactly to the inverted channel matrix,  $T^{-1}(\omega)$ . When we examine the system as a whole when a matched filtering is implemented at the receiver, denoted as  $H(\omega)$ , we are left with the total system as being  $\tilde{W}(\omega) = H(\omega)T^{-1}(\omega)T(\omega)H(\omega) = H(\omega)IH(\omega)$ , where  $I$  represents the identity matrix.

It is apparent that the matched filtering effects affect the final system multiplicatively twice, and therefore hampers system performance. The use of an anti-aliasing filter, however, instead yields a final identical to  $\check{W}(\omega) = H(\omega)I$ , and therefore reduces such effects from the super Gaussian filter.

For the simulations in this work, precoding was performed upon a block of 128 bits at a bit rate of 1 Gb/s, rather than bit-by-bit in the frequency domain or via adopting a new pulse shape in the time domain. Adopting a new pulse shape for each of the three modes involves obtaining the impulse response of each coefficient in precoding matrix. However, tests to implement a new pulse when the precoder was exactly equal to the inverted transmission matrix in the frequency domain failed to retain the original transmitted bit streams. This is believed to be due to the fact that the inverse channel matrix is determined by taking the inverse with respect to matrix arithmetic rather than frequency, which is not intuitive to obtain. Additionally, bit-by-bit precoding in the frequency domain proved unrealizable as well due to issues with sizing a precoder to fit across a single bit properly.

By transmitting specific bit sequences, we can exploit critical magnitude and phase information for each coefficient in the MMF channel matrix and subsequently develop the appropriate precoder, denoted as the matrix  $A$ . The development of the precoder, including the mathematical basis and simulation results under various conditions, when applied to the low coupling scenario is explained in Section 4.1. The simulation performance of the precoder adapted for the frequency flat case and under differing conditions is examined in Section 4.2.

## 4.1 Precoding Filter Training Scheme

We propose sending specific bit sequences for each mode in order to extract the magnitude and phase information for each coefficient,  $T_{ij}$ , in the frequency flat channel matrix, described by the matrix  $T(\omega)$  at the center frequency. We begin by initializing the precoder matrix,  $A$ , to the matrix described by (4.1) below, where  $\omega_c$  represents the center frequency.

$$A = \begin{pmatrix} 1 & 0 & 0 \\ 0 & e^{j\Delta\beta(\omega_c)L} & 0 \\ 0 & 0 & e^{j\Delta\beta(\omega_c)L} \end{pmatrix} \quad (4.1)$$

The initialization matrix of  $A$  draws upon the ideal propagation matrix described by (3.2) in the previous chapter. The idea is to eliminate most of the phase shifting caused by the transmission matrix at the center frequency and, therefore, retain a precoder that will remove such effects more effectively.

Subsequently, we transmit each bit sequence of the form  $\underline{x} = (b_0 \ b_1 \ b_2)^T$  through the fiber, yielding an output of the form  $\underline{y}^{(b_0 \ b_1 \ b_2)} = TAx$ . The next phase of the process is to construct an estimate, denoted  $Q$ , of the channel matrix, where  $Q = TA$ , given the output of each bit sequence sent. Considering the noiseless case for mathematical simplicity, the output of the fiber post-square law detection when a generic bit sequence,  $\underline{x} = (b_0 \ b_1 \ b_2)^T$ , is shown in (4.2) below.

$$\underline{z} = \begin{pmatrix} |Q_{11}b_0 + Q_{12}b_1 + Q_{13}b_2|^2 \\ |Q_{21}b_0 + Q_{22}b_1 + Q_{23}b_2|^2 \\ |Q_{31}b_0 + Q_{32}b_1 + Q_{33}b_2|^2 \end{pmatrix} \quad (4.2)$$

Substituting various combinations of bits for  $b_0$ ,  $b_1$ , and  $b_2$  allows us to compute the magnitude and phase components of the transmission matrix via subsequent algebraic manipulations of the output bit sequences. The magnitude components can be determined by transmitting a sequence containing a single high bit. For instance, sending the sequence

$\underline{x} = (0\ 0\ 1)^T$  yields  $\underline{z}^{(0\ 0\ 1)} = (|Q_{13}|^2\ |Q_{23}|^2\ |Q_{33}|^2)^T$ , and taking the square root of  $\underline{y}^{(0\ 0\ 1)}$  provides the exact magnitudes of the channel matrix. The magnitudes of the other six coefficients are given by  $\underline{z}^{(0\ 1\ 0)} = (|Q_{12}|^2\ |Q_{22}|^2\ |Q_{32}|^2)^T$  and  $\underline{z}^{(1\ 0\ 0)} = (|Q_{11}|^2\ |Q_{21}|^2\ |Q_{31}|^2)^T$  when  $\underline{x} = (0\ 1\ 0)^T$  and  $\underline{x} = (1\ 0\ 0)^T$  respectively.

The nine phase components of the transmission matrix are determined by setting two bits of the training sequence high, producing the phase difference between two coefficients for a single row in the transmission matrix. The phase is considerably much more difficult to estimate accurately. Ergo, we assume knowledge of the  $T_{11}$  and  $T_{22}$  coefficients and utilize this information to determine the phases of the other seven coefficients in the matrix. We begin first by transmitting a sequence with two high bits, such as  $x = (1\ 0\ 1)^T$  as an example. Substitution into (4.2) yields (4.3) below.

$$z^{(1\ 1\ 0)} = \begin{pmatrix} |Q_{11}b_0 + Q_{12}b_2|^2 \\ |Q_{21}b_0 + Q_{22}b_2|^2 \\ |Q_{31}b_0 + Q_{32}b_2|^2 \end{pmatrix} = \begin{pmatrix} |Q_{11}|^2 + |Q_{12}|^2 + 2|Q_{11}||Q_{12}|\cos(\phi_{(11)} - \phi_{(12)}) \\ |Q_{21}|^2 + |Q_{22}|^2 + 2|Q_{21}||Q_{22}|\cos(\phi_{(21)} - \phi_{(22)}) \\ |Q_{31}|^2 + |Q_{32}|^2 + 2|Q_{31}||Q_{32}|\cos(\phi_{(31)} - \phi_{(32)}) \end{pmatrix} \quad (4.3)$$

The phase differences can be computed by eliminating the magnitude coefficients through algebraic expressions developed from the outputs  $\underline{z}^{(0\ 1\ 0)}$ ,  $\underline{z}^{(1\ 0\ 0)}$ , and  $\underline{z}^{(0\ 0\ 1)}$ . In the example given in (4.3), the phase difference term between  $Q_{11}$  and  $Q_{13}$  is isolated via (4.4) below. The notation  $z^{(1\ 0\ 1)}(1)$  indicates that the first row of  $z^{(1\ 0\ 1)}$  is accessed.

$$(\phi_{(11)} - \phi_{(12)}) = \arccos\left(\frac{z^{(1\ 1\ 0)}(1) - z^{(1\ 0\ 0)}(1) - \underline{z}^{(0\ 1\ 0)}(1)}{2\sqrt{\underline{z}^{(0\ 1\ 0)}(1) \cdot z^{(1\ 0\ 0)}(1)}}\right) \quad (4.4)$$

The six other phase difference components are determined by sending and manipulating sequences  $\underline{x} = (1\ 0\ 1)^T$  and  $\underline{x} = (1\ 1\ 0)^T$ , which yields  $z^{(1\ 0\ 1)}$  and  $z^{(1\ 1\ 0)}$  respectively, in a similar fashion. The other eight phase differences are shown in (4.5) through (4.12).

$$(\phi_{(12)} - \phi_{(13)}) = \arccos \left( \frac{\underline{z}^{(0\ 1\ 1)}(1) - \underline{z}^{(0\ 0\ 1)}(1) - \underline{z}^{(0\ 1\ 0)}(1)}{2\sqrt{\underline{z}^{(0\ 0\ 1)}(1) \cdot \underline{z}^{(0\ 1\ 0)}(1)}} \right) \quad (4.5)$$

$$(\phi_{(11)} - \phi_{(13)}) = \arccos \left( \frac{\underline{z}^{(1\ 0\ 1)}(1) - \underline{z}^{(0\ 0\ 1)}(1) - \underline{z}^{(1\ 0\ 0)}(1)}{2\sqrt{\underline{z}^{(0\ 0\ 1)}(1) \cdot \underline{z}^{(1\ 0\ 0)}(1)}} \right) \quad (4.6)$$

$$(\phi_{(21)} - \phi_{(22)}) = \arccos \left( \frac{\underline{z}^{(1\ 1\ 0)}(2) - \underline{z}^{(1\ 0\ 0)}(2) - \underline{z}^{(0\ 1\ 0)}(2)}{2\sqrt{\underline{z}^{(0\ 1\ 0)}(2) \cdot \underline{z}^{(1\ 0\ 0)}(2)}} \right) \quad (4.7)$$

$$(\phi_{(22)} - \phi_{(23)}) = \arccos \left( \frac{\underline{z}^{(0\ 1\ 1)}(2) - \underline{z}^{(0\ 0\ 1)}(2) - \underline{z}^{(0\ 1\ 0)}(2)}{2\sqrt{\underline{z}^{(0\ 0\ 1)}(2) \cdot \underline{z}^{(0\ 1\ 0)}(2)}} \right) \quad (4.8)$$

$$(\phi_{(21)} - \phi_{(23)}) = \arccos \left( \frac{\underline{z}^{(1\ 0\ 1)}(2) - \underline{z}^{(0\ 0\ 1)}(2) - \underline{z}^{(1\ 0\ 0)}(2)}{2\sqrt{\underline{z}^{(0\ 0\ 1)}(2) \cdot \underline{z}^{(1\ 0\ 0)}(2)}} \right) \quad (4.9)$$

$$(\phi_{(31)} - \phi_{(32)}) = \arccos \left( \frac{\underline{z}^{(1\ 1\ 0)}(3) - \underline{z}^{(1\ 0\ 0)}(3) - \underline{z}^{(0\ 1\ 0)}(3)}{2\sqrt{\underline{z}^{(0\ 1\ 0)}(3) \cdot \underline{z}^{(1\ 0\ 0)}(3)}} \right) \quad (4.10)$$

$$(\phi_{(32)} - \phi_{(33)}) = \arccos \left( \frac{\underline{z}^{(0\ 1\ 1)}(3) - \underline{z}^{(0\ 0\ 1)}(3) - \underline{z}^{(0\ 1\ 0)}(3)}{2\sqrt{\underline{z}^{(0\ 0\ 1)}(3) \cdot \underline{z}^{(0\ 1\ 0)}(3)}} \right) \quad (4.11)$$

$$(\phi_{(31)} - \phi_{(33)}) = \arccos \left( \frac{\underline{z}^{(1\ 0\ 1)}(3) - \underline{z}^{(0\ 0\ 1)}(3) - \underline{z}^{(1\ 0\ 0)}(3)}{2\sqrt{\underline{z}^{(0\ 0\ 1)}(3) \cdot \underline{z}^{(1\ 0\ 0)}(3)}} \right) \quad (4.12)$$

The final task is to estimate the individual phase components for each channel matrix coefficient. Given that we have knowledge of the  $T_{11}$  and  $T_{22}$  phases, computing the individual phase becomes a trivial matter of addition or subtraction depending on the relationship between the two phases. In total, the phases for each coefficient in  $Q$  are computed through the set of equations highlighted in (4.13) through (4.21)

$$\phi_{11} = \angle T_{11} \quad (4.13)$$

$$\phi_{12} = \phi_{11} - (\phi_{(11)} - \phi_{(12)}) \quad (4.14)$$

$$\phi_{13} = \phi_{12} + (\phi_{(12)} - \phi_{(13)}) \quad (4.15)$$

$$\phi_{22} = \angle T_{22} \quad (4.16)$$

$$\phi_{21} = \phi_{22} - (\phi_{(21)} - \phi_{(22)}) \quad (4.17)$$

$$\phi_{23} = \phi_{22} - (\phi_{(22)} - \phi_{(23)}) \quad (4.18)$$

$$\phi_{33} = \angle T_{11} + 2 \cdot \angle T_{22} \quad (4.19)$$

$$\phi_{32} = \phi_{33} + (\phi_{(32)} - \phi_{(33)}) \quad (4.20)$$

$$\phi_{31} = \phi_{33} + (\phi_{(31)} - \phi_{(33)}) \quad (4.21)$$

Once the magnitude and phase components are obtained, we create the  $Q$  as shown in (4.22) below as an estimate of  $T$ .

$$Q = \begin{pmatrix} |Q_{11}|e^{j\phi_{11}} & |Q_{12}|e^{j\phi_{12}} & |Q_{13}|e^{j\phi_{13}} \\ |Q_{21}|e^{j\phi_{21}} & |Q_{22}|e^{j\phi_{22}} & |Q_{23}|e^{j\phi_{23}} \\ |Q_{31}|e^{j\phi_{31}} & |Q_{32}|e^{j\phi_{32}} & |Q_{33}|e^{j\phi_{33}} \end{pmatrix} \quad (4.22)$$

Particularly when noise is present, we propose that the bit streams be transmitted  $N$  times per coherence interval to generate  $N$   $Q$  matrices. Subsequently, all of the  $Q$  matrices are

averaged, signified by  $Q_t$ , and used to update the precoder,  $A$ . Once  $Q_t$  is established, the precoder is updated via (4.23), and ultimately results.

$$A := A(Q_t)^{-1} \quad (4.23)$$

The accuracy of the training algorithm and (4.15) was evaluated by computing the mean squared error (MSE) between the precoder and the inverse of the channel matrix at the carrier frequency, which was used to train the precoder. The SNR was set to 1 dB and 100 trials were performed. The results are shown in Figure 4.2.

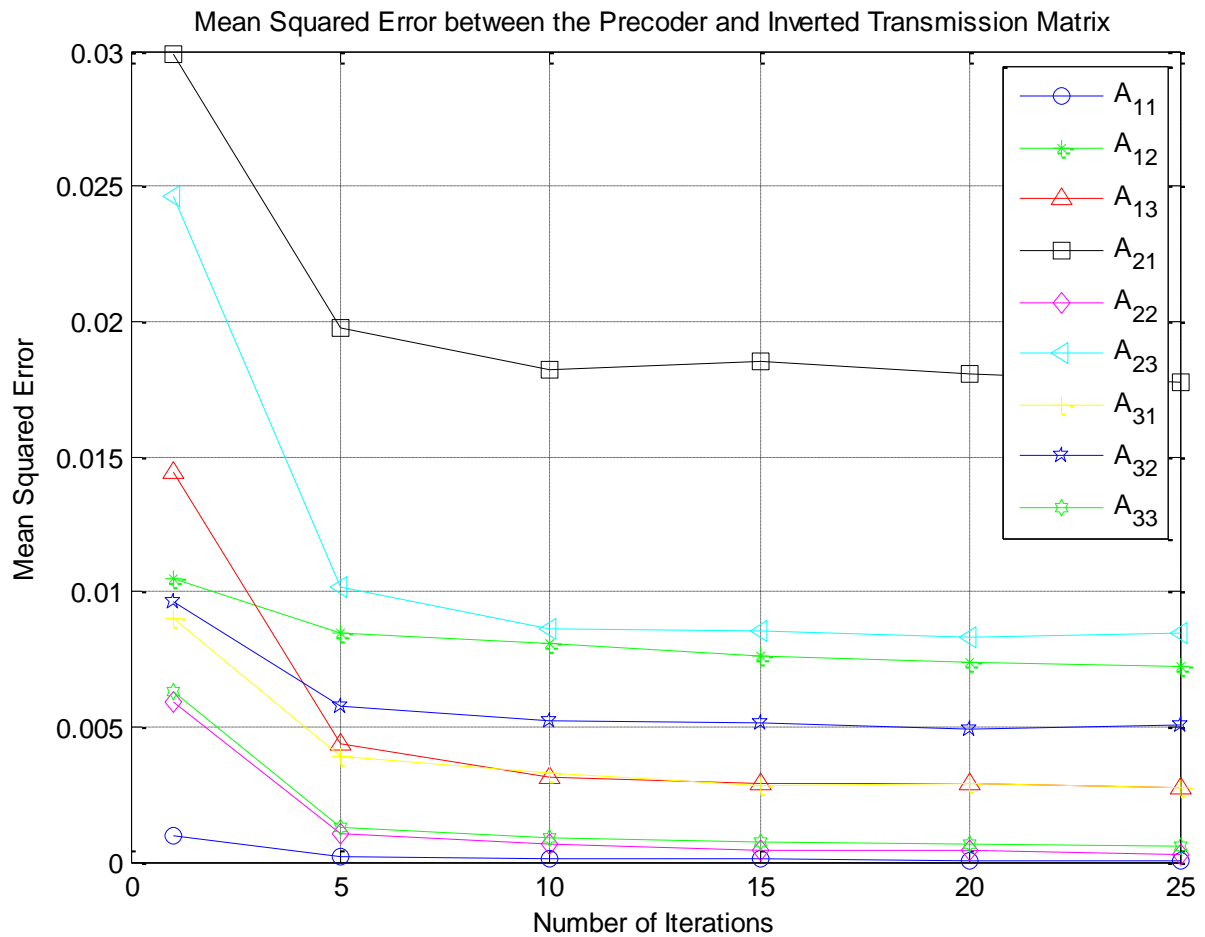


Figure 4.2: The MSE between the precoder and the inverse of the center frequency transmission matrix.

Figure 4.2 shows that the training algorithm works quite well across all iterations and provides an accurate estimate of the ideal precoder, which is the inverse of the transmission matrix used for training. Additionally, we note that the best estimate arises when ten iterations are performed of the algorithm.

## 4. 2 Simulation Results

The iterative precoder training scheme was applied to a low coupling frequency flat system. The channel matrix used for training a single precoder was the matrix located at the carrier frequency of the system. The full transmission matrix computed by the model described in Chapter 3 was used for testing. Five hundred trials were performed and averaged for all tests and performance curves generated. Each trial generated 128 bits for testing at a bit rate of 1 Gb/s.

Each test was examined in the presence of AWGN incurred during detection of each mode. SNR in this instance can be described as the ratio of the optical input power of the first mode, which was determined to be on average roughly -19 dB, to the electrical noise at the receiver. The natural first step is to compare the unfiltered MMF performance versus the precoder trained with a single iteration, which is shown in Figure 4.3.

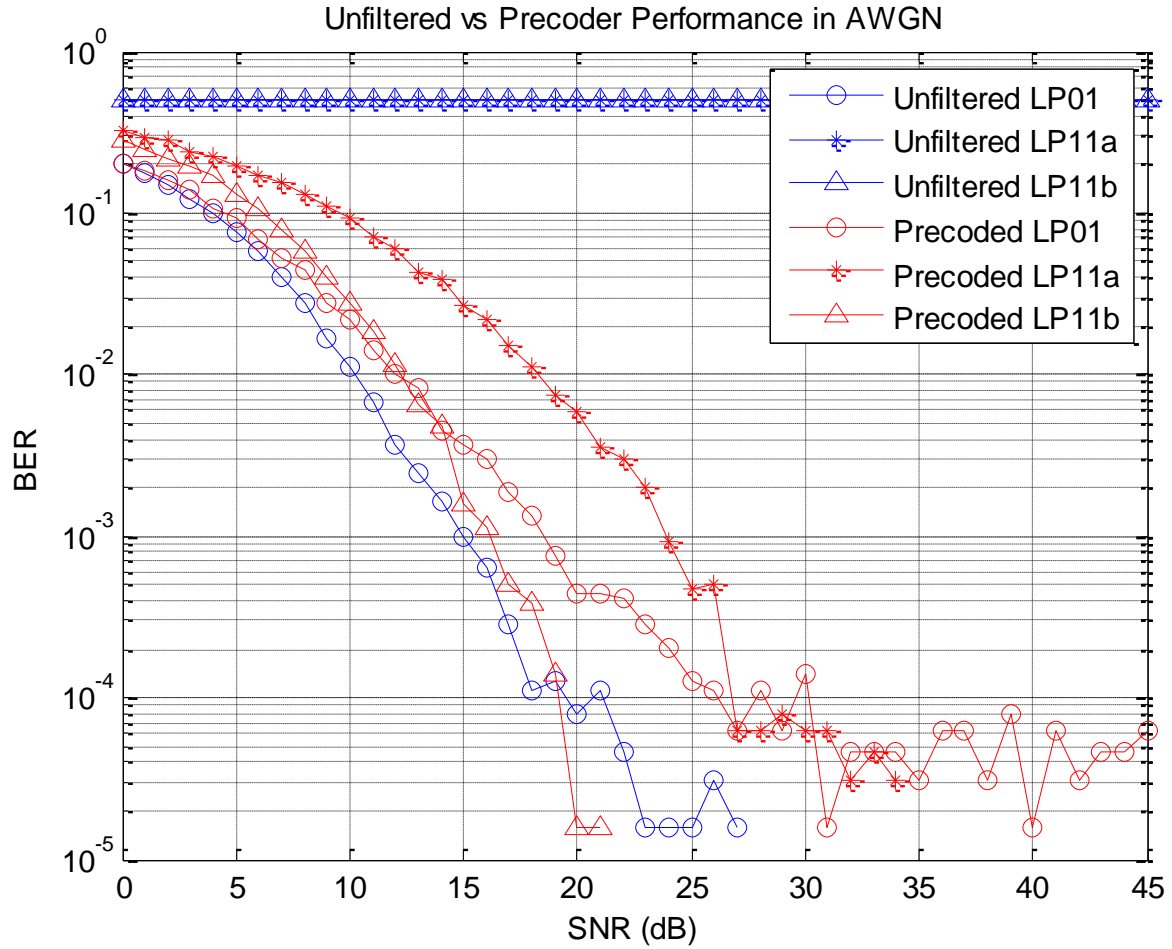


Figure 4.3: The performance curves of the unfiltered and precoded MMFs versus SNR.

It is clear from Figure 4.3 that the precoder brings great performance improvements from the unfiltered system, particularly at high SNR levels. In the unfiltered case, the secondary modes have near consistent unsatisfactory performance levels across all SNR values, while the fundamental mode contains errors at low SNRs. The secondary modes have high BERs due to the fact that they share a propagation constant, meaning that the two modes travel at the same rate and, thus, are highly coupled with each other. On the other hand, the fundamental mode travels at a vastly different rate and, thus, does not exchange power with the other modes in the fiber.

The performance of the precoder for the three propagating modes reduces the BER considerably for the secondary modes at higher SNR levels, despite introducing some error into the LP01 mode. The precoder does not perform as well at low SNR values due to the impact of random noise upon the magnitude and phase estimations. An SNR of roughly 25 dB yields a precoder that reduces noise considerably when a single iteration is used to train the precoder.

The precoder developed was also compared to the ideal precoding matrix, which is exactly the inverse of the transmission matrix at the center frequency. Figure 4.4 illustrates the performance of the ideal and the generated precoders.

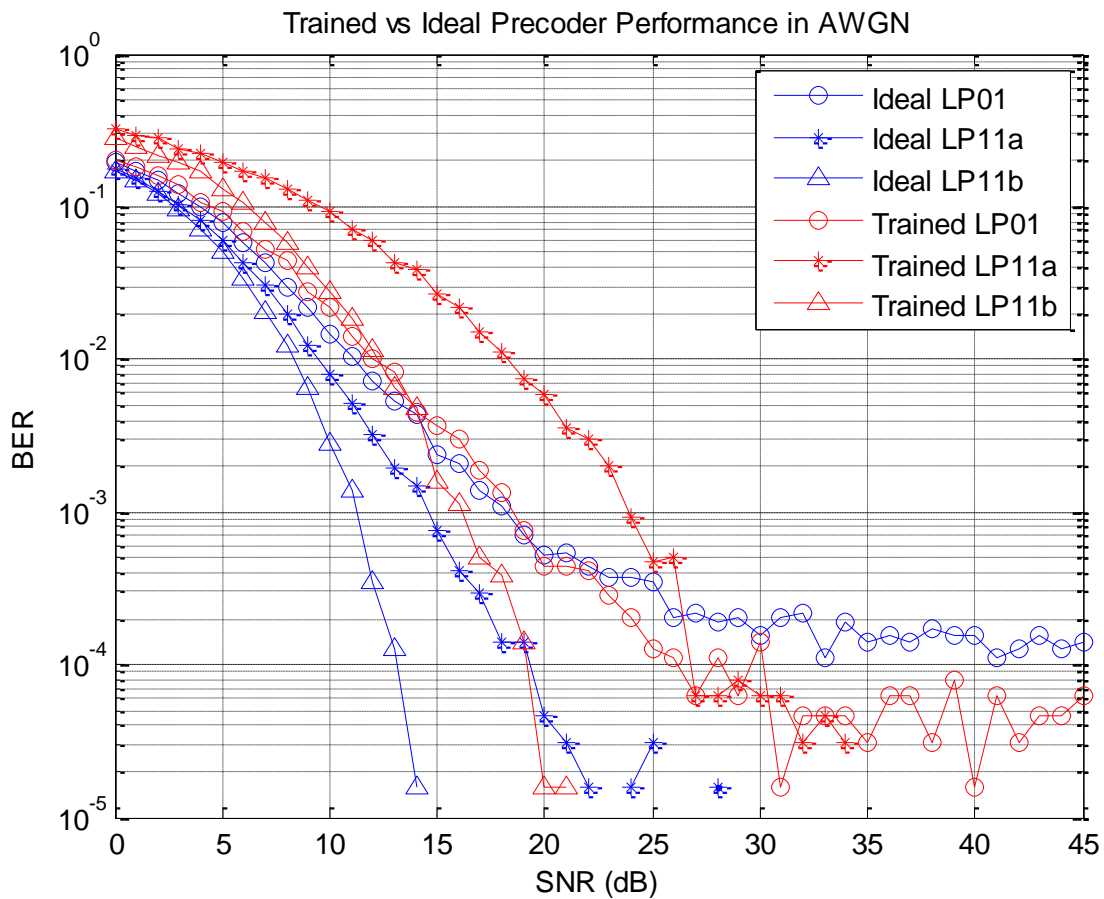


Figure 4.4: Performance curves comparing the generated and ideal precoders.

From Figure 4.4, we note that the ideal precoder boasts considerably lower errors for all three modes across all SNR levels, in contrast to the generated precoder. However, as the SNR

increases to 25 dB and beyond, the performance of the generated precoder nearly matches that of the ideal precoder for all three modes and is an encouraging indicator of the precoder's effectiveness.

In order to improve precoder tolerance to AWGN, each bit sequence was sent  $N$  times to achieve  $N$  different  $Q$  matrices. Subsequently, the final  $Q_t$  matrix is the average of all the  $Q$  matrices obtained in training and used to create  $A$  via (4.14). Since the LP01 mode does not suffer from significant errors in the unfiltered frequency flat scenario with respect to the channel itself, performance was gauged with respect to the secondary LP11 modes. Performance in the presence of noise when the number of iterations was varied is shown in Figures 4.5 and 4.6 for the LP11a and LP11b modes respectively.

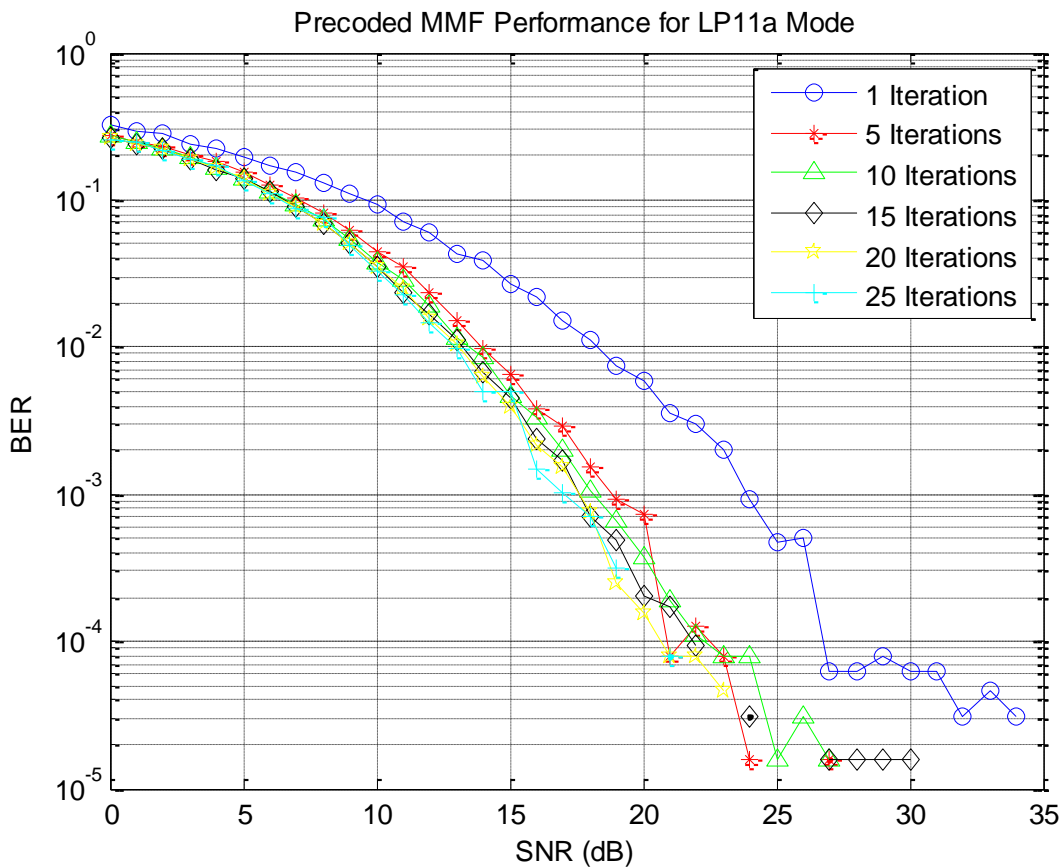


Figure 4.5: LP11a precoder performance vs SNR as a function of the number of iterations.

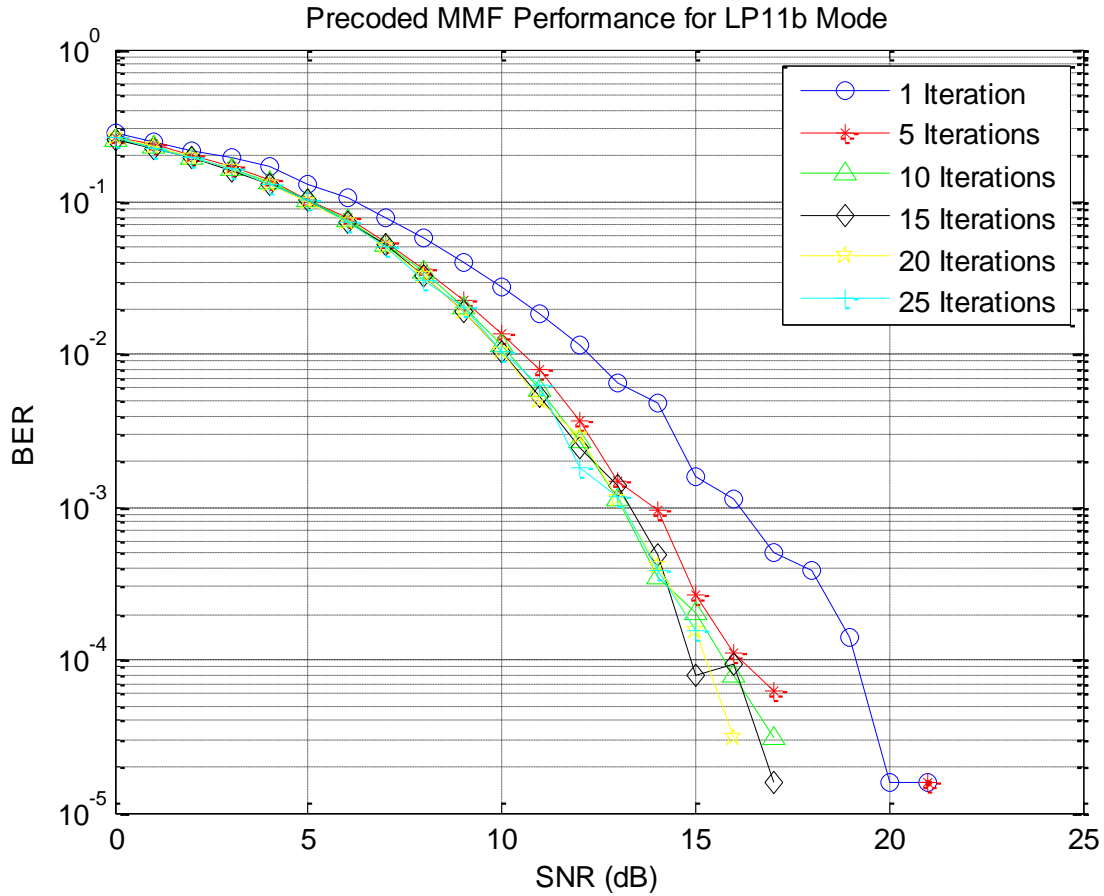


Figure 4.6: LP11b precoder performance vs SNR as a function of the number of iterations.

Increasing the number of training iterations per coherence interval dramatically improves precoder robustness when exposed to AWGN. As noted in Figures 4.5 and 4.6, an increase in training iterations to five yields performance improvements, but subsequent increases in performance are limited, which is supported by Figure 4.2. This is due to the inherent limitation of OOK modulation in the presence of AWGN.

Finally, the precoder performance was evaluated when the amount of coupling was increased from 0.01 in increments to 0.05. The performance curves were generated at an SNR of 20 dB and 5 iterations were performed to produce the precoder. The results are contained in Figure 4.7.

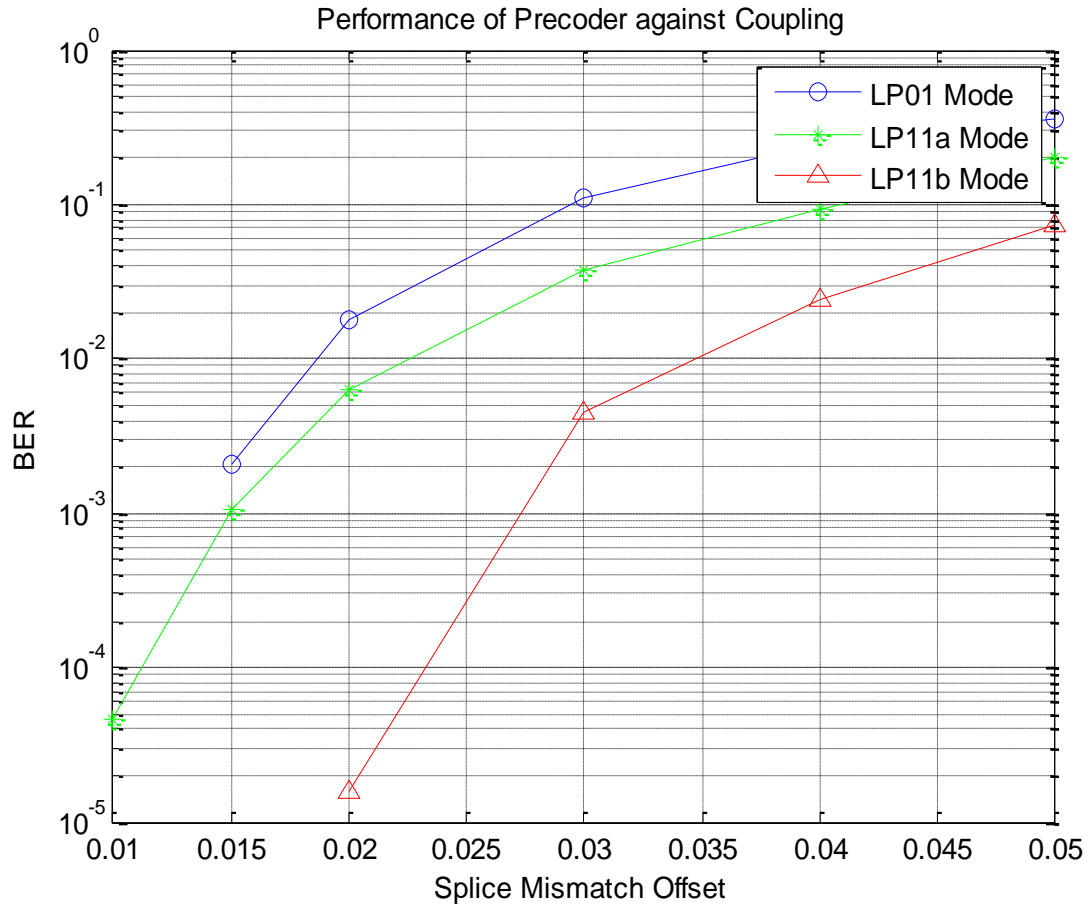


Figure 4.7: Precoder performance across various levels of splice mismatching.

As noted in Figure 4.7, the precoder training algorithm is geared toward MMFs with low coupling and splice mismatching and, therefore, is frequency flat in nature. As the splice mismatch offset increase and the channel becomes frequency selective in nature, we see that the BER increases steadily to unsatisfactory levels, and is unusable for actual data transmission. The precoder developed in this work is better suited for frequency flat MMFs, and the development of a precoder to alleviate frequency selective scenarios is left as future work with recommendations made in Chapter 5.

### 4.3 Chapter Summary

In Chapter 4, we presented a precoder suitable for operation in the low coupling regime. By sending specific training bit sequences, we can obtain CSI regarding magnitude and phase and use it to create an appropriate precoder. As shown in Figure 4.2 and 4.3, we note that the precoder created is a relatively close estimate of the inverse of the transmission matrix, with many coefficients having MSE values of only several tenths. Figure 4.4 shows a clear improvement in performance from that of the unfiltered MMF with low coupling, particularly with regards to the secondary modes. When AWGN is present, increasing the number of iterations allows us to create a generalized precoder that reduces error significantly across both secondary modes examined. Finally, as coupling increases in the MMF, the precoder become less effective, which raises questions with regards to creating a precoder that is more tolerant to a frequency selective system.

# Chapter 5 – Summary and Future Work

## 5.1 Thesis Summary and Conclusions

This thesis presents the concept of multimode optical fiber and provides a method to enhance its performance via precoding at the transmitter. The classic single mode optical fiber system is reaching its fundamental capacity limit. Although attempts have been made to saturate single mode fiber performance, capacity gains prove to be minimal at best, forcing research to overhaul fiber optic communications. Multimode fiber, which is typically used in short-haul applications, has potential to increase capacity significantly, but is greatly hindered by modal dispersive and coupling effects caused by several modes propagating at once. In order for MMFs to become a viable solution for medium- or long-haul applications, researchers have classically turned toward applying MIMO post-processing wireless techniques or launching specific modes of the fiber.

The key concept of this thesis is to apply a pre-distortion technique to alleviate channel dispersive effects prior to transmission. While precoding has been heavily investigated and utilized in other communication media, little work has been done in applying such a method to MMFs. An iterative training scheme involving the transmission of specific bit sequences is proposed in order to exploit specific information about the channel, which is subsequently utilized to create an appropriate precoder. As noted in Chapter 4, the precoder produced when iterated multiple times produces a relatively accurate description of the original transmission matrix and is rather tolerant to noise. However, the precoder examined in this thesis is only applicable to the very low coupling scenario, where the system is said to be frequency flat.

With a coupling of 0.01, where the coupling loss is approximately 0 dB for each mode, the precoder developed in this thesis was able to recreate the inverse of the transmission matrix accurately and reduced BERs significantly to usable levels. Increasing the number of iterations in the presence of noise allowed us to yield performance improvements of several decibels in the cases of the secondary modes, particularly when 5 or more iterations were performed. When applied to MMFs with splice mismatching values of 0.01 to 0.05, the performance of the precoder decreased, showing that the method is only usable for MMFs with low coupling and, hence, frequency flat in nature.

## 5.2 Future Work

Multiple recommendations are suggested for the continuation of this work. It is necessary for the relationship between the phases to be investigated further to eliminate the assumptions of knowledge regarding the phases of two of the diagonal coefficients. A suggestion is to potentially send sequences containing values other than '1' and '0', such as '-1' or the imaginary component 'i'. Sending different sequences could eliminate the need for any assumptions on phase and allow us to obtain values on both phases explicitly.

It is clear that a precoder needs to be developed to bring meaningful improvements to the frequency selective case, where a single precoder is not sufficient. Several concepts were explored to correct the frequency selective case, one of which was to create a precoding matrix for every frequency of the transmission matrix to correct a block of bits sent at a time. However, issues were encountered when computing the magnitude and phase components necessary to create the precoder. A potential fix may be to alter the inputs of the training bit streams. Rather

than transmitting purely ones or zeros, a sinusoid operating at the frequency in question could be utilized instead to exploit the characteristics of the channel at a given point.

Should a proper precoder per frequency be found, it is then necessary to determine if a downsampled sequence can be used to train the precoder for the sake of computational complexity. Subsequently, the precoder can be resampled at the transmitter to pre-correct each bit stream properly. Several methods of resampling exist, and a recommendation is to examine whether this can be performed while maintain signal integrity. Finally, a technique that can retain a precoder to be applied bit-by-bit is suggested with the thought of computational complexity in mind.

# Bibliography

- [1] R. Tkach. "Scaling Optical Communications for the Next Decade and Beyond." Bell Labs Technical Journal, vol. 14, no.1, 2010.
- [2] G. P. Agrawal. *Fiber-Optic Communication Systems*. Wiley, fourth edition, 2010.
- [3] C. DeCusatis. *Fiber Optic Data Communication*. Academic Press, 2002.
- [4] R. Lingle. "Capacity Increase in Optical Fiber Links." *Wireless and Optical Communications Conference*, May 14-15, 2010.
- [5] K. Appaiah, S. Vishwanath, and S. Bank. "Vector Intensity-Modulation and Channel State Feedback for Multimode Fiber Optic Links." *IEEE Transactions on Communications*, vol. 61, no. 7, pp. 2958-2969, July 2013.
- [6] A. Juarez, C. Bunge, S. Warm, and K. Petermann. "Perspectices of principal mode transmission in mode-division-multiplex operation." *Optics Express*, vol. 20, no. 13, June 2012.
- [7] S. Arik, J. Kahn, and K. Ho. (2014, February). "MIMO Signal Processing for Mode-Division Multiplexing" *IEEE Signal Processing Magazine*. 31 (2), pp. 25-34. Available: <http://ieeexplore.ieee.org/stamp/stamp.jsp?tp=&arnumber=6739233> [March 19, 2014].
- [8] M. Nazarathy and A. Agmon. "Coherent Transmission Direct Detection MIMO Over Short-Range Optical Interconnects and Passive Optical Networks." *Journal of Lightwave Technology*, vol. 26, no. 14, pp. 2037-2045, July 15, 2008.
- [9] A. Agmon and M. Nazarathy. "Broadcast MIMO over multimode optical interconnects by modal beamforming." *Optics Express*, vol. 15, no. 20, October 1, 2007.
- [10] A. Snyder and J. Love. *Optical Waveguide Theory*. New York, NY: Chapman Hall, 1983.
- [11] K.-P. Ho and J. M. Kahn, "Mode Coupling and its Impact on Spatially Multiplexed Systems", in *Optical Fiber Telecommunications VI*, I. P. Kaminow, T. Li and A. E. Willner, Eds., Elsevier, Amsterdam, 2013 (*Invited Chapter*).
- [12] A. Juarez, E. Krune, S. Warm, C. Bunge, and K. Petermann. "Modeling of Mode Coupling in Multimode Fibers With Respect to Bandwidth and Loss." *Journal of Lightwave Technology*, vol. 32, no. 8, pp. 1549-1558, April 15, 2014.
- [13] H. Unger. *Planar Optical Waveguides and Fibres*. Oxford, UK: Clarendon Press, 1977.
- [14] N. Bikhazi, M. Jensen, and A. Anderson. "MIMO Signaling over the MMF Optical Broadcast Channel with Square-Law Detection." *IEEE Transactions on Communications*, vol. 57, no. 3, pp. 614-617, March 2009.

[15] P. Kairouz and A. Singer. "MIMO Communications over Multi-Mode Optical Fibers: Capacity Analysis and Input-Output Coupling Schemes." Online. Available: <http://arxiv.org/pdf/1304.0422v1.pdf> . April 2013.

[16] S. Arik, J. Kahn, and K. Ho. "Effect of Mode Coupling on Signal Processing Complexity in Mode-Division Multiplexing." *IEEE Journal of Lightwave Technology*, vol. 31, no. 3, pp. 423-431, February 2013.

[17] A. Agmon and M. Nazarathy. "Broadcast MIMO over multimode optical interconnects by modal beamforming." *Optics Express*, vol. 15, no. 20, October 1, 2007.